



Variability of BL
turbulence

V. Maurer et al.

This discussion paper is/has been under review for the journal Atmospheric Chemistry and Physics (ACP). Please refer to the corresponding final paper in ACP if available.

Observed spatial variability of boundary-layer turbulence over flat, heterogeneous terrain

V. Maurer¹, N. Kalthoff¹, A. Wieser¹, M. Kohler¹, and M. Mauder²

¹Institut für Meteorologie und Klimaforschung (IMK-TRO), Karlsruher Institut für Technologie (KIT), Karlsruhe, Germany

²Institut für Meteorologie und Klimaforschung (IMK-IFU), Karlsruher Institut für Technologie (KIT), Garmisch-Partenkirchen, Germany

Received: 03 June 2015 – Accepted: 11 June 2015 – Published: 02 July 2015

Correspondence to: V. Maurer (vera.maurer@kit.edu)

Published by Copernicus Publications on behalf of the European Geosciences Union.

Title Page

Abstract

Introduction

Conclusions

References

Tables

Figures



Back

Close

Full Screen / Esc

Printer-friendly Version

Interactive Discussion



Abstract

In spring 2013, extensive measurements with multiple Doppler lidar systems were performed. The instruments were arranged in a triangle with edge lengths of about 3 km in a moderately flat, agriculturally used terrain. For six mostly cloud-free convective days, vertical velocity variance profiles were compared for the three locations. On the average over all considered cases, differences between variances at different sites were about three times higher than between those derived from measurements by different lidars at the same site. For all investigated averaging periods between 10 min and 4 h, the differences were not significant on the average when considering the statistical error. However, statistically significant spatial differences were found in several individual cases. These could not be explained by the existing surface heterogeneity.

In some cases, nearby energy balance stations provided surface fluxes that were not suitable for scaling the variance profiles. Weighted-averaged values proved to be more applicable, but even then, the scaled profiles showed a large scatter for each location. Therefore, it must be assumed that the intensity of turbulence is not always well-determined by the local heat supply at the Earth's surface. Instead, a certain dependency of turbulence characteristics on mean wind speed and direction was found: thermals were detected that travelled from one site to the other with the mean wind when the travel time was shorter than the large-eddy turnover time. At the same time, no thermals passed for more than two hours at a third site that was located perpendicular to the mean wind direction in relation to the first two sites. Subsidence prevailing in the surroundings of thermals advected with the mean wind can thus partly explain significant spatial variance differences existing for several hours.

1 Introduction

The vertical velocity variance, $\overline{w'^2}$, is one of the relevant parameters describing the turbulent structure of the convective boundary layer (CBL). Measurements of $\overline{w'^2}$ have

Variability of BL turbulence

V. Maurer et al.

Title Page

Abstract

Introduction

Conclusions

References

Tables

Figures



Back

Close

Full Screen / Esc

Printer-friendly Version

Interactive Discussion



Variability of BL turbulence

V. Maurer et al.

Title Page

Abstract

Introduction

Conclusions

References

Tables

Figures

◀

▶

◀

▶

Back

Close

Full Screen / Esc

Printer-friendly Version

Interactive Discussion



been analyzed for several decades (e.g. Wyngaard et al., 1971; Panofsky and Maz-
zola, 1971; Kaimal et al., 1976; Young, 1988). Most of these early investigations were
based on aircraft observations. Later, radar wind profiler (e.g., Eymard and Weill, 1988;
Angevine et al., 1994; Eng et al., 2003) and more recently, Doppler lidar measurements
(e.g. Lothon et al., 2009; Hogan et al., 2009; Ansmann et al., 2010; Lenschow et al.,
2012) became available for studying vertical velocity characteristics in the CBL. Both
in-situ aircraft measurements and ground-based remote sensing have advantages and
disadvantages: as aircraft observations are expensive, data are usually available for
a small number of flight levels only. The measurements must cover a certain distance,
i.e. flight legs must be long enough, to meet the requirements of turbulent statistics
(Lenschow and Stankov, 1986; Lenschow et al., 1994), so that the turbulence charac-
teristics on the different levels are not available simultaneously. Ground-based remote
sensing observations provide turbulent statistics on different levels at the same time for
time periods of typically one hour or even longer. However, even if it is assumed that
temporal and spatial integration are comparable, i.e. that time can be transformed into
space via the mean wind speed, lidar measurements are representative of a restricted
region only.

In the part of the CBL where buoyant production dominates over the shear produc-
tion of turbulent kinetic energy, turbulent mixing is supposed to be driven mainly by the
heat supply at the Earth's surface. Deardorff (1970a) proposed that for situations with
sufficient thermal instability, vertical velocity fluctuations could be scaled by the convec-
tive velocity w_* . Warner (1972), Willis and Deardorff (1974) and Caughey and Palmer
(1979) were among the first to present scaled variance profiles, based on laboratory
experiments as well as aircraft measurements performed over mainly homogeneous
terrain. Large eddy simulations (LES) confirmed the empirical profiles (e.g. Deardorff,
1974; Moeng, 1984; Hadfield et al., 1991). Different fit functions were proposed by
Kaimal et al. (1976), Lenschow et al. (1980), or Sorbjan (1988, 1989), which reveal
a considerable uncertainty. Hogan et al. (2009), e.g., found that scaled variance pro-
files derived from lidar measurements at one particular site displayed a case-to-case

Variability of BL turbulence

V. Maurer et al.

Title Page

Abstract

Introduction

Conclusions

References

Tables

Figures



Back

Close

Full Screen / Esc

Printer-friendly Version

Interactive Discussion



variability that was about as large as the scatter of the fit functions given by Lenschow et al. (1980) and Sorbjan (1986), which had been derived from aircraft measurements. Hence, the uncertainty or representativeness of point measurements is very relevant and becomes even more important for heterogeneous terrain.

Different studies addressed the representativeness of point measurements of the surface energy balance (e.g. Mahrt, 1998; Steinfeld et al., 2007) and examined sampling errors made by aircraft measurements (e.g. Lenschow and Stankov, 1986; Schröter et al., 2000). Lenschow et al. (1994) considered general statistical errors that should be taken into account when calculating turbulence statistics. To our knowledge, no investigation specifically addressed the statistical errors made for simultaneously performed point measurements of vertical turbulence profiles.

During the High Definition Clouds and Precipitation for Climate Prediction (HD(CP)²) observational prototype experiment (HOPE) performed in April and May 2013 in the Lower Rhine region in Germany, Doppler lidars were deployed in a triangle in an agriculturally used, moderately flat terrain (Fig. 1). The length of about 3 km of the three edges had been chosen such that the measurements could be assumed to be independent. As it was supposed that most processes in the CBL scale with its depth (e.g. Deardorff, 1970a; Willis and Deardorff, 1974), the lengths had to be larger than the CBL depth of 1–2 km. On the other hand, the locations had to be close enough to be situated within the area of the given surface heterogeneity. The aims of this study were (1) to compare the vertical velocity variance profiles at the three sites, i.e. to investigate the spatial variability of CBL turbulence and with this, to assess the representativeness of point measurements over patchy terrain; (2) to analyze the conditions of the time periods with statistically significant spatial variance differences in more detail; (3) to investigate the effect of w_* -scaling on the spread of profiles of $\overline{w'^2}$ by using spatially averaged values of w_* or those derived from stations near to the lidar locations; and (4) to determine the impact of the averaging time on spatial variance differences.

The paper is structured as follows: in the next section, the observations and the measurement setup are described. Section 3 presents the computation of the verti-

Variability of BL turbulence

V. Maurer et al.

Title Page

Abstract

Introduction

Conclusions

References

Tables

Figures



Back

Close

Full Screen / Esc

Printer-friendly Version

Interactive Discussion



cal velocity variances and considered errors and includes considerations regarding the normalization procedure. In Sect. 4, the main results are presented and discussed. This comprises the spatial comparison of the variances, the investigation of surface and atmospheric conditions during periods with statistically significant differences of the variances, and the discussion of possible influencing factors. Finally, Sect. 5 summarizes the main findings.

2 Overview of the measurements

2.1 Measurement site and instruments

The HOPE measurement area was located near Forschungszentrum Jülich, in the north of a low mountain range (Eifel), with two larger open-pit coal mines (up to 10 km wide) and several smaller wooded areas in the vicinity. All instruments considered here were located within an agriculturally used area near the villages of Hambach and Niederzier (Fig. 1). The diagonals of the individual fields with various crops are roughly between 100 and 500 m. As part of HOPE, the Karlsruhe advanced mobile observation platform KITcube (Kalthoff et al., 2013) was installed. Most of the KITcube instrumentation was operated at Hambach (50.897° N/6.464° E, 110 m.m.s.l.). Additionally, instruments were installed at a second site, called Wasserwerk (50.891° N/6.430° E, 96 m.m.s.l.), 2.6 km west of Hambach. For this study, Doppler lidar data from a site near Selhausen (50.869° N/6.451° E, 105 m.m.s.l.) and energy balance data from eddy-covariance stations (Graf et al., 2010) of the Terrestrial Network of Observatories (TERENO; Zacharias et al., 2011) were applied as well. The instruments whose data are used here are briefly described below.

2.1.1 Doppler lidars at three sites

At Hambach, a 1.6 μm heterodyne Doppler lidar (WindTracer “WTX” with an Er:YAG laser, Lockheed Martin Coherent Technologies, Inc.) was deployed. The lidar measures

**Variability of BL
turbulence**

V. Maurer et al.

Title Page

Abstract

Introduction

Conclusions

References

Tables

Figures

◀

▶

◀

▶

Back

Close

Full Screen / Esc

Printer-friendly Version

Interactive Discussion



the radial wind velocity via the Doppler shift of radiation scattered at aerosol particles. Mean horizontal wind speed profiles can be calculated with the VAD algorithm (Brown-
ing and Wexler, 1968). Applying the vertical stare mode yields vertical velocity w with
a time resolution of 1 s from about 375 m above ground level (a.g.l.) to the top of the
boundary layer and partly above, depending on the aerosol concentration as well as
on the measurement setup. Technically, a higher data rate of 10 Hz would be possible,
but a temporal resolution of 1 Hz is considered the optimal setting for the vertical stare
mode, as it ensures higher signal-to-noise ratios by longer averaging. The effective
range-gate resolution is about 60 m (Träumner et al., 2011). The measurements are
mainly restricted to the cloud-free atmosphere, because lidars only partly penetrate
clouds. In order to cover the range between the top of the surface layer and the lowest
measurement heights of WTX, a Doppler lidar (WLS7-V2, Leosphere, hereafter called
WLS7) with a wavelength of 1.5 μm was used. Applying the VAD mode yields the wind
profile from 40 m a.g.l. up to about 400 m a.g.l. with a temporal resolution of 1.6 s to
10 min and a vertical range resolution of 20 m. As for WTX, operation of the system in
the vertical stare mode allows for the direct detection of vertical velocity. In combination
with the WindTracer WTX at Hambach, a full vertical coverage of vertical velocity from
the top of the surface layer up into the entrainment zone results.

Two Doppler lidars (a 2 μm lidar called WindTracer “HYB” with a Tm:LuAG
laser/Lockheed Martin CT, and WLS200/Leosphere) were operated at the Wasserwerk.
Apart from the different laser transmitters, the HYB has similar system settings as
the WTX. The Doppler lidar at Selhausen, the third site, was a Stream Line manufac-
tured by HALO Photonics Ltd. (Pearson et al., 2009, hereafter called HALO), which
measures with a range-gate length of 18 m (Eder et al., 2015). In contrast to the Wind-
Tracer systems having a laser pulse of high energy, the HALO and the WLS200 op-
erate in a “low-pulse energy/high-pulse rate mode” and they can resolve the lowest
hundreds of meters a.g.l. An overview of the lidar instruments at the different locations
is also given in Table 1. The variability of the threshold of signal-to-noise ratio taken for
filtering noisy data for the different instruments is also related to the different technical

specifications. The measurement frequency of 1 Hz was the same for all Doppler lidars and the measurement settings were chosen such that vertical velocity data were available at intervals of 25 m for the WindTracer systems as well as for the systems from Leosphere. For the WindTracer systems, this setup causes an overlap of the effective range gates. The data of HALO were interpolated to the same heights.

As all heights used in this study will be in m a.g.l., we will omit the adjunct “a.g.l.” in the following sections.

2.1.2 Energy balance stations

The energy balance stations measure solar and reflected irradiance, long-wave incoming and outgoing radiation, soil heat, sensible heat, latent heat, and momentum fluxes. For the turbulent fluxes, temperature, humidity, and wind speed are measured with an ultrasonic anemometer/thermometer and a fast infrared hygrometer at a height of 4 m. All turbulent fluxes used in this study were calculated for time intervals of 30 min using the eddy-covariance software package TK3.11 of Mauder and Foken (2011) and Mauder et al. (2013). Altogether, data of five energy balance stations were used: two energy balance stations of KITcube that were co-located with the lidar instruments at Hambach and at the Wasserwerk site and three TERENO stations at Niederzier, Selhausen, and Ruraue (Fig. 1).

2.1.3 Additional instruments at Hambach

To obtain vertical profiles of temperature, humidity, wind speed, and wind direction, the KITcube radiosonde system (DFM-09, Graw) was operated at Hambach. On 18 days selected as intensive operation periods (IOPs), radiosondes were launched at 2-hourly intervals. On all other days, launches were done at least at 11:00 and 23:00 UTC. A microwave radiometer (HATPRO, Radiometer Physics GmbH) was also operated at Hambach. The instrument detects thermal radiation emitted by atmospheric components. From these data, for example time series of integrated water vapor (IWV) can

Variability of BL turbulence

V. Maurer et al.

Title Page

Abstract

Introduction

Conclusions

References

Tables

Figures



Back

Close

Full Screen / Esc

Printer-friendly Version

Interactive Discussion



be derived with high accuracy (Pospichal and Crewell, 2007). An additional ultrasonic anemometer was installed on a tower and measured wind components and virtual temperature at a height of 30 m. Finally, a ceilometer (CHM 15k, Jenoptic) measured cloud-base heights.

2.2 Turbulent surface fluxes

An overview of the daily averaged Bowen ratios (ratio of daily averaged sensible heat flux to daily averaged latent heat flux, using 09:00–15:00 UTC) indicates that the values were very high (up to 4) for some stations until 6 May 2013, but below one at all stations after that date (Fig. 2a). The Bowen ratio was below one at Selhausen and Ruraue during all the time so that spatial heterogeneity within the respective area of about 5 km × 5 km existed in April until early May. The rain gauge measurements at the Wasserwerk (Fig. 2b) reveal that there was much less rainfall during this period than after 6 May. From the land-surface point of view, the whole measurement period may be divided into a drier period with considerable spatial heterogeneity and a wetter period with less heterogeneity. Similar differences of Bowen ratio between a wet and a dry period were found during the field experiment LITFASS-2003, which also took place in an area dominated by agricultural land use (Beyrich and Mengelkamp, 2006).

In order to derive spatially representative values of sensible heat flux, an average of flux measurements was calculated by weighting each station with the fraction of the respective land-use class in the considered area (Fig. 1). The land-use map was available at 15 m × 15 m horizontal resolution and the land-use classes were combined to the following three categories: bare soil, crops, and meadow/forest, with fractions of 70.2, 22.8, and 7.1 %, respectively. As the growth of vegetation was not yet advanced in spring 2013, the fluxes of Niederzier were considered to be representative of bare soil, even though the station was located in a field of sugar beets. The stations Selhausen and Wasserwerk (crops) were assigned to the second land-use class and Ruraue and Hambach (meadow) to the third one. As the fraction of bare soil was by far the highest and the Bowen ratio at Niederzier was high during the drier period, the

Variability of BL turbulence

V. Maurer et al.

Title Page

Abstract

Introduction

Conclusions

References

Tables

Figures



Back

Close

Full Screen / Esc

Printer-friendly Version

Interactive Discussion



weighted-averaged flux also is higher during the drier than during the wetter period (Fig. 2a).

2.3 Selected days

On six days with mainly cloud-free CBL conditions, at least one lidar at each site was configured for w measurements: 18, 20, 22, and 24 April as well as 04 and 19 May. Here, the variance profiles for all of these days were analyzed. From the radiosoundings, mean CBL conditions were estimated for these six days (Table 2): on four of the six days, the main regime was governed by westerly to southwesterly flow. On 20 April, the mean wind direction was from northeast and on 19 May, it varied between northeast to north in the CBL, while it was from the east directly above the CBL. As indicated by microwave radiometer measurements, the IWV was moderately high on most days and much higher on 24 April. Incoming shortwave radiation, as measured by a pyranometer network operated by TROPOS (Leipzig), naturally increased from 18 April to 19 May. At the same time, the spatial standard deviation of incoming radiation, in combination with ceilometer data and cloud camera images, revealed the existence of some CBL clouds on 18 April, of cirrus clouds at about 8 km on 24 April, and of altocumulus clouds at about 5 km on 19 May. In comparison to the other days, however, the maximum sensible heat flux was reduced on 19 May because this was the only day falling into the wetter period. The height of the capping inversion of the CBL was also lowest on 19 May, while it was highest on 18 April. As indicated by the temporal evolution of temperature profiles of the radiosondes for 18 April (not shown), a neutrally stratified residual layer was present between 800 and 1400 m at 09:00 UTC above the mixed layer. When the boundary layer grew into this neutral layer, its height increased abruptly from 700 m at 09:00 UTC to 1600 m at 11:00 UTC. This also may have contributed to the formation of some boundary-layer clouds on this day as the sudden mixing throughout the deepened CBL led to a cooling of the former residual layer.

Variability of BL turbulence

V. Maurer et al.

Title Page

Abstract

Introduction

Conclusions

References

Tables

Figures

⏪

⏩

◀

▶

Back

Close

Full Screen / Esc

Printer-friendly Version

Interactive Discussion



3 Vertical velocity measurements and variance calculations

3.1 Characteristics of vertical velocity data

As an example, vertical velocity measurements from 11:00–13:00 UTC on 20 April at the three sites are shown for comparison (Fig. 3). Up- and downdrafts with a maximum vertical velocity of more than 2.5 m s^{-1} , which are typical of convective boundary layers, were observed at all sites. The thermals lasted for several minutes and rose up to 1200 m during this time period. The isolines of 283–285 K of potential temperature (Fig. 3b) display the height of the inversion layer at 1200 m, which also agrees with the measurement heights of the lidars WTX and HALO (Fig. 3b and c). The HYB yielded measurements up to 1500 m (Fig. 3a). This is due to the averaging of a higher number of laser pulses so that the signal-to-noise ratio is still above the selected threshold (Table 1) at heights where the aerosol concentration is much lower. It can also be seen that the w measurements of the WLS7 and WLS200 for the lowest 400 m are subjectively consistent with the measurements above (Fig. 3a and b).

For a first analysis of the time series, power density spectra of w were calculated at different heights for the instruments at Hambach (Fig. 4a). Additionally, the spectrum of w measurements by an ultrasonic on a 30 m tower is given and can be compared with those of WLS7 at the lowest range gate (60 m). At low frequencies of about 10^{-3} to 10^{-2} Hz (i.e. time periods of about 2–15 min), the energy is highest for all range gates except for the lowest one. Maximum turbulent energy for the considered time series can be found at 400 m height, as indicated by the integral spectrum (Fig. 4b). At the lowest given range gate and for the ultrasonic measurement, maximum energy is shifted towards higher frequencies (0.01 to 0.1 Hz) and smaller time periods (10 s to 2 min), respectively. Besides, as discussed by Frehlich et al. (1998) or Brugger et al. (2015) for example, it is obvious that in the inertial subrange, the energy of the lidar spectra decreases faster than the theoretical $-2/3$ -slope, i.e. for frequencies higher than about 0.1 Hz for the WTX (400 m and above) and about 0.3 Hz for WLS7 (60 and 200 m). Even if the measurement frequencies of 1 Hz of the two lidar systems would be high enough

Title Page

Abstract

Introduction

Conclusions

References

Tables

Figures



Back

Close

Full Screen / Esc

Printer-friendly Version

Interactive Discussion



Variability of BL
turbulence

V. Maurer et al.

Title Page

Abstract

Introduction

Conclusions

References

Tables

Figures



Back

Close

Full Screen / Esc

Printer-friendly Version

Interactive Discussion



to register fluctuations on these scales, the sampling frequency is restricted due to the spatial averaging of the lidar pulses. This affects the absolute values of variance, as can be seen in the integral spectra: while the contribution to the total energy still increases up to the highest frequency resolved by the measurement frequency for the WLS7 spectra, this is not the case for the WTX spectra. The total energy or variance, respectively, is therefore higher at 200 m than at 900 m. Apart from that, the spectra of WLS7 show some artefacts at the highest frequencies, which were also observed by Carbajo Fuertes et al. (2014), for example. This is presumably the signature of an aliasing effect. As the effect of missing variance contributions at high frequencies due to the spatial averaging is found for all lidar systems and as the main aim of our investigation is an intercomparison of lidar measurements at different locations, this effect will be neglected below.

The integral spectra indicate that the largest contributions to the variance ($> 50\%$) lie in the frequency range of 2×10^{-3} to 10^{-2} Hz (Fig. 4b). Based on the spectra, the peak frequency $f_{p,w}$ lying within this range was estimated for all days. From $f_{p,w}$, the time and length scales on which the turbulent energy contained in the vertical motions is highest were calculated. They varied for the considered days between five and eight minutes or 2–2.7 km, respectively (Table 2). Additionally, scales can be estimated from the autocorrelation function of w : it becomes negative at a certain time interval and will have a second maximum (and further maxima), if a dominant periodic fluctuation exists. The interval, at which the second maximum can be discerned does then correspond to the repetition frequency of the up- or downward motions. This repetition frequency often corresponds to the peak wavelength. The values are slightly larger than those estimated from the spectra, but they confirm that the peak wavelength is about 3 km (Table 2). This means that the energy-containing length scale of the turbulent motions in the CBL was much larger during HOPE than the length scale of the surface heterogeneity, which is several 100 m at the maximum.

Instead of the calculation via the integrated spectrum, the w'^2 profiles were determined directly from the time series. For a validation of both computation methods, the

hourly variances for all considered instruments and all six days calculated by both methods were compared for the 600 m range gates and were found to be in good agreement, with a mean relative deviation of 3 %.

3.2 Errors considered for variance calculations

As in Träumner et al. (2011), the variances were corrected for uncorrelated random noise using a technique proposed by Lenschow et al. (2000). Additionally, the statistical error was considered as described by Lenschow et al. (1994). This method is based on the separation of the random and the systematic error (Appendix A).

Even if the signal noise is considered, we cannot be sure that different instruments can provide identical measurements, especially if they are from different manufacturers and are based on different technical principles like HALO and WLS200 compared to the WindTracer systems. Therefore, both WLS200 and HYB were operated at the Wasserwerk in the vertical stare mode on 20, 22, and 24 April, so that the w measurements of the two lidar systems could be compared directly. The cross correlation function between the two w time series on 20 April was calculated for measurement heights between 400 and 1000 m (not shown). The highest correlations (> 0.8) can be found between 600 and 800 m. As for the autocorrelation functions, an oscillation between positive and negative values is observed for increasing time lags, symmetrically for positive and negative ones. For 18 and 22 April, the maximum correlations are 0.88 and 0.95, respectively. This means that the two measurements were not perfectly the same on all days, but sufficiently well correlated to possibly yield similar statistics. The variance differences resulting from the different devices will be taken into account for the spatial comparisons in Sect. 4.4.

Finally, another error that may have an influence is the missing contribution to turbulent energy in the higher frequency part of the spectrum due to the vertical averaging of the lidar measurements. As explained above, this error will be neglected here, as it would lead to higher variances at all stations and not change the spatial differences.

Variability of BL turbulence

V. Maurer et al.

Title Page

Abstract

Introduction

Conclusions

References

Tables

Figures



Back

Close

Full Screen / Esc

Printer-friendly Version

Interactive Discussion



3.3 Scaling of variance profiles

According to Lenschow et al. (1980) and Sorbjan (1989), vertical profiles of $\overline{w'^2}$ can be normalized and best fitted by

$$\frac{\overline{w'^2}}{w_*^2} = 1.8 \left(\frac{z}{z_i} \right)^{2/3} \left(1 - 0.8 \frac{z}{z_i} \right)^2 \quad \text{and} \quad \frac{\overline{w'^2}}{w_*^2} = 1.17 \left(\frac{z}{z_i} \right)^{2/3} \left(1 - \frac{z}{z_i} \right)^{2/3}, \quad (1)$$

5 respectively. The convective velocity scale is defined as

$$w_* = \left(z_i \frac{g}{\theta_{v,0}} \overline{w' \theta_v'} \Big|_0 \right)^{1/3}, \quad (2)$$

with the CBL height z_i , the gravitational acceleration g , the temporal mean of virtual potential temperature at the surface $\overline{\theta_{v,0}}$, and the kinematic sensible heat flux at the surface, $\overline{w' \theta_v'} \Big|_0$. For the sensible heat flux, either the weighted-averaged heat flux
10 (see Sect. 2) or the fluxes measured by the energy balance stations next to the lidar instruments can be used here.

For z axis scaling as well as to calculate w_* , the CBL height has to be determined. At least, three different methods are in use, depending on the available measurement systems (cf. Emeis et al., 2008; Träumner et al., 2011, and references therein): (1)
15 determining the CBL capping inversion from radiosonde profiles, (2) estimating the top of the aerosol layer from lidar backscatter data, and (3) calculating the top of CBL convection from profiles of the vertical velocity variance. While the first two methods can be regarded as proxies for the CBL depth, the third method is a direct one. Tucker et al. (2009) systematically investigated the determination of the CBL height using
20 variance profiles and found that a threshold value to which the variance decreases was the best objective criterion. Träumner et al. (2011) determined this threshold value for

Title Page

Abstract

Introduction

Conclusions

References

Tables

Figures



Back

Close

Full Screen / Esc

Printer-friendly Version

Interactive Discussion



Variability of BL turbulence

V. Maurer et al.

Title Page

Abstract

Introduction

Conclusions

References

Tables

Figures



Back

Close

Full Screen / Esc

Printer-friendly Version

Interactive Discussion



the HYB for several field campaigns and found that a value of $0.16 \text{ m}^2 \text{ s}^{-2}$ gave the best results. However, the threshold value was not applicable to all of the profiles here. With this in mind and as the z_i values derived by methods (1) and (2) showed a good agreement (dashed lines and black dots in Fig. 5), method (2) was chosen, because it provides values for periods when no radiosoundings are available. The values of w_* resulting from using z_i determined by method (2) and the weighted-averaged fluxes are also given in Fig. 5 (gray lines). A comparison of diurnal maximum values of $\overline{w'^2}$ and w_* is included in Table 2. From w_* , a convective time scale $t_* = z_i/w_*$ can be derived that describes how long it takes to transport an air parcel from the ground to the top of the CBL.

4 Spatial and temporal differences of vertical velocity variances

4.1 Profiles of variance and skewness: examples for 20 April

Examples of profiles of w variance calculated for four instruments at the three locations are shown in Fig. 6. The given times always indicate the end of the averaging period of one hour. As described by Deardorff (1974) or Lenschow et al. (1980), the variance profiles display a maximum at a height of about one third of the convective boundary layer (the top of the CBL is between 1000 and 1400 m on 20 April, Fig. 5) and a decrease above. The profiles in Fig. 6 are not normalized so that the diurnal evolution may be observed: variances are small at 10:00 UTC (12:00 LT), increase to maximum values at about 12:00–14:00 UTC and decrease subsequently. Above a local minimum indicating the top of the CBL, an increase of variance can be seen in several profiles (e.g. 13:00–16:00 UTC profiles of HYB at about 1500 m, Fig. 6a). These higher values lie in and above the capping inversion of the CBL (Fig. 3b) and can presumably be attributed to the existence of gravity waves there.

As already shown by the comparison of vertical velocity measurements of the smaller WLS7 and of WTX (Fig. 3), the combined variance profiles fit well at the transition

Variability of BL turbulence

V. Maurer et al.

Title Page

Abstract

Introduction

Conclusions

References

Tables

Figures

◀

▶

◀

▶

Back

Close

Full Screen / Esc

Printer-friendly Version

Interactive Discussion



height from one instrument to the other (Fig. 6d). The maximum variance is sometimes located at low heights that are not covered by HYB or WTX (for example, at 11:00 UTC in Fig. 6c), indicating the usefulness of the combination of different lidar systems with complementary ranges. The variance profiles derived from the measurements of HYB and WLS200 (Fig. 6a and b) do not agree in all details, as indicated by the calculated cross correlations, but the profiles are much more similar to each other than to the profiles from the other two sites in terms of structure, temporal evolution, and absolute values.

Additionally, profiles of skewness $\left(\overline{w'^3}/\overline{w'^2}^{3/2}\right)$ were analyzed (Fig. 6). Positive skewness is usually expected in the CBL and means strong, narrow updrafts and weaker, broader downdrafts. On 20 April, values of skewness are positive within the CBL. They confirm the existence of a well-mixed boundary layer, as they illustrate a net upward transport of variance (according to the variance budget equation of Stull, 1988) and with this, of turbulent energy. This means that the turbulent energy is mainly created at the surface, i.e. by buoyancy.

4.2 Spatial comparison of variances

One noticeable difference between the hourly variance profiles at the three locations on 20 April (Fig. 6) is the diurnal cycle: while maximum variance occurs at 12:00 UTC at Wasserwerk and Selhausen, it occurred at 14:00 UTC at Hambach. The question is whether this is statistically significant or not. To investigate this, the height of maximum variance, z_{\max} , was determined for all days and all hourly variance profiles. It was encountered between $0.1 z_j$ and $0.5 z_j$. A maximum variance $\overline{w'^2}_{\max}$ was then calculated by vertical averaging of each profile over a height range of $z_{\max} \pm 250$ m. The statistical errors were determined for the same height range. The time series of $\overline{w'^2}_{\max}$ for the three locations are shown in Fig. 7. The difference of $\overline{w'^2}_{\max}$ between Wasserwerk and Hambach on 20 April for the 12:00 UTC period is not significant when considering the

statistical error. However, for some time periods, as for example for 11:00 and 15:00–16:00 UTC on 18 April, 11:00 and 14:00 UTC on 20 April or 12:00 UTC on 24 April, significant differences between the individual locations can be discerned.

For 20 April, 13:00–14:00 UTC for example, differences are also obvious in the time series of vertical velocity (Fig. 8): at Hambach, where the variance is the highest, about 5–6 periods with convective cells can be distinguished. As the peak energy resides at the lowest frequencies (Fig. 4), as it is associated with the largest turbulence elements, the high variance at Hambach for this hour is attributable to the multiple occurrence of convective cells. At Wasserwerk, the variance is slightly lower than at Hambach because less convective cells passed the site. At Selhausen, the variance is smallest and the least convective cells occurred. Obviously, the spatial variance differences are attributable to the different numbers of convective cells at the three sites that are only about 3 km apart. For the three selected periods with significant differences, we will investigate now whether these differences can be explained by surface conditions.

4.3 Influence of surface conditions

Spatial differences of the state of the CBL may be caused by spatially heterogeneous surface conditions. For the days investigated here, positive values of skewness confirm that the strength of turbulence is dominated by surface-based buoyancy-driven convection (exemplarily shown for 20 April in Fig. 6). The spatial heterogeneity of the buoyancy flux at the surface may be considered by scaling the variance profiles with w_*^2 . Generally, surface heterogeneity as observed during the drier period (Fig. 2) may be caused by heterogeneous surface characteristics such as land use and soil moisture, which influence the partitioning of available energy into sensible and latent heat. On the other hand, heterogeneity also can result from the available energy itself, which can be modified strongly by the occurrence of clouds. As shown in Sect. 2.3, clouds actually occurred on three of the six selected days.

Variability of BL turbulence

V. Maurer et al.

Title Page

Abstract

Introduction

Conclusions

References

Tables

Figures



Back

Close

Full Screen / Esc

Printer-friendly Version

Interactive Discussion



4.3.1 Scaled profiles: selected periods

For the three selected time periods on 18, 20, and 24 April when spatial differences were observed, scaled profiles with the corresponding error bars are given in Fig. 9. For each site, the surface sensible heat flux from a nearby energy balance station was used for calculating w_* and, thus, for scaling. Two energy balance stations were located near Selhausen: The energy balance station of Niederzier was about 1 km north of Selhausen which may be relatively far away, but the land-use class was the same as at the lidar location. The station called SE1 was closer, but the land-use class there differed and the flux was very low, even lower than at Ruraue (Figs. 2 and 10), which was located in a meadow close to a river. Hence, Niederzier was chosen for scaling the variances of Selhausen.

For all time periods, at least two profiles still show statistically significant differences after applying the w_* -scaling. For 18 April, 15:00 UTC (Fig. 9a), the difference between Hambach and Wasserwerk becomes even more obvious than without scaling. This means that the spatial differences cannot be explained by the surface heterogeneity. The reason becomes obvious when looking at the net radiation and surface sensible heat flux for the three selected time periods (Fig. 10): on 18 April at 15:00 UTC, the w variance is the highest at Selhausen and lower at Hambach as well as at Wasserwerk (Fig. 7). If local sensible heat fluxes were responsible for the spatial differences of the turbulence between 14:00–15:00 UTC, the spatial flux differences would be similar. However, the flux is highest at Hambach (Fig. 10) so that the scaled variance was the lowest. At Niederzier, the flux is slightly lower and much lower at Wasserwerk. Consequently, the differences of the sensible heat flux can not explain the variance differences. Moreover, net radiation (Fig. 10) shows that some clouds occur on this day and from cloud camera images, it is known that also boundary-layer clouds are present. These clouds do not cause considerably temporal variation in the sensible heat flux data, but they can certainly influence the variance profiles (e.g. Neggers et al., 2003).

Title Page

Abstract

Introduction

Conclusions

References

Tables

Figures



Back

Close

Full Screen / Esc

Printer-friendly Version

Interactive Discussion



Variability of BL turbulence

V. Maurer et al.

Title Page

Abstract

Introduction

Conclusions

References

Tables

Figures



Back

Close

Full Screen / Esc

Printer-friendly Version

Interactive Discussion



On 20 April, 14:00 UTC (Fig. 9b), the variance is highest at Hambach and lower at Wasserwerk as well as at Selhausen (Fig. 7). However, the surface sensible heat flux is equally high at the three locations. At the same time, the net radiation shows little variability ($< 20 \text{ W m}^{-2}$) at this time. Thus, the surface forcing does not display large differences between the three locations, which explains why a scaling using the fluxes from the nearby stations does not remove the spatial differences of variances.

On 24 April, 12:00 UTC (Fig. 9c), the variance at Selhausen is significantly lower than at Hambach and Wasserwerk (Fig. 7) but again, the spatial differences between the fluxes can not explain this difference. The flux is highest at Niederzier (Fig. 10) so that the scaled variance profile for Selhausen becomes very low compared to the scaled profiles at the other two locations.

As regards the selected examples, it must be concluded that the heterogeneous surface conditions can not explain the statistically significant differences of the w variances.

4.3.2 Scaled profiles: whole data set

To investigate the impact of the scaling on all available w variance profiles in a systematic way, all profiles were normalized by both averaged scaling (using weighted-averaged fluxes for w_*) and local scaling (using fluxes of nearby stations as in Sect. 4.3.1). It is assumed that the local diurnal cycle of the energy input as well as local differences from day to day can be taken into account better by local scaling than by the averaged one. Therefore, also the question is addressed whether the spread between the profiles at each individual location is smaller for the locally scaled profiles. 19 May, which is the only day falling into the wetter period with less surface heterogeneity (see Sect. 2.2), is excluded from the following analysis.

In Sect. 4.3.1, Niederzier had been chosen before for scaling because of the land-use class, but proved not to be completely suitable. A different land-use class is given at SE1, but the station is closer. Consequently, both were used for scaling the variance profiles from Selhausen (Fig. 11g and h). As Niederzier is a bare-soil station with rela-

Variability of BL turbulence

V. Maurer et al.

Title Page

Abstract

Introduction

Conclusions

References

Tables

Figures



Back

Close

Full Screen / Esc

Printer-friendly Version

Interactive Discussion



tively high sensible heat fluxes (Fig. 10), i.e. a high Bowen ratio, and SE1 is characterized by a low Bowen ratio, large differences are found between the two normalizations: the maximum values of mean normalized variance are 0.31 and 0.70, respectively. For the averaged scaling, by contrast, the maximum value of the mean scaled variance at Selhausen is 0.35 (Fig. 11c), which is more similar to the mean values of $\overline{w'^2}/w_*^2$ at Hambach and Wasserwerk (0.38 and 0.37, respectively, Fig. 11a and b). This means that in comparison to the scaled variances at the other locations, the surface sensible heat flux at Niederzier is too high for scaling the variances from Selhausen and SE1 too low with respect to the observed CBL turbulence.

The mean profiles using averaged scaling (thick lines in Fig. 11a–c) display a vertical behavior that is similar to the profile of Lenschow et al. (1980, Fig. 11d), but with a lower maximum ($\overline{w'^2}/w_*^2 < 0.4$). The similarity of these three mean profiles implies that also the mean profiles of w variances (without scaling) are similar at the three locations. For WTX at Hambach (Fig. 11a and e), the difference between averaged and local scaling is very small for both mean values (mean maximum of $\overline{w'^2}/w_*^2 = 0.39$ for local scaling) as well as the scatter of the profiles. This means that the energy balance station at this site provides values which are representative of the considered domain. For HYB (Fig. 11b and f), the locally scaled profiles exhibit a smaller scatter than those generated by averaged scaling.

To investigate the dependence of the spread between the profiles on the scaling method, correlation coefficients were determined: (1) between the w variance values at $0.35 z_j$ ($\overline{w'^2}_{0.35}$) and w_*^2 , calculated with weighted-averaged fluxes (averaged scaling, Fig. 12a), and (2) between $\overline{w'^2}_{0.35}$ and w_*^2 , calculated with the respective fluxes used for local scaling (Fig. 12b). In case of 1), the squared correlation coefficient R^2 is 0.25 for Hambach and 0.32 for Wasserwerk; in case of 2), the correlation is slightly higher than in case (1) for Hambach ($R^2 = 0.28$) and strongly for Wasserwerk ($R^2 = 0.58$). For Selhausen, the squared correlation coefficient is higher in case (1) than in case (2) when using the fluxes from Niederzier or Selhausen (0.21 or 0.29, respectively, compared

Variability of BL turbulence

V. Maurer et al.

Title Page

Abstract

Introduction

Conclusions

References

Tables

Figures

◀

▶

◀

▶

Back

Close

Full Screen / Esc

Printer-friendly Version

Interactive Discussion



to 0.33 for case 1). This means that the local scaling is not preferable for Selhausen when using either of the available energy balance measurements. For Hambach, local scaling is only slightly better than averaged scaling, but local scaling is clearly better for Wasserwerk. The correlations are all significant according to a t-test on a 1 %-level, except for $R^2 = 0.21$ (Fig. 12b). However, the values also indicate that the explained variances (concerning the temporal evolution of the $\overline{w'^2}_{0.35}$, hereafter called “temporal variance” to avoid ambiguity) are about 30 % in all cases but in one. Deardorff (1970b, 1974) showed that $\overline{w'^2}_{0.35} = a w_*^2$ and found values of a between 0.37 and 0.44 which were derived from both numerical experiments and different observations. Here, a is 0.32–0.44 for the averaged w_*^2 values and 0.36–0.47 for the local ones. This variation is not negligible and, in combination with high portions of unexplained temporal variances, it implies that either the intensity of turbulence in the CBL also depends on parameters other than the heat supply at the Earth’s surface or that the uncertainty of the calculated scaling parameters is too large. Spatial variability of z_i may be larger than assumed so that the values of w_* using z_i derived from variance measurements at Hambach are not valid for Wasserwerk and Selhausen. However, the normalized variance profiles mainly display a minimum at $z/z_i = 1$ (Fig. 11). For HALO, the profiles break off at $z/z_i \approx 0.95$, which may indicate a lower z_i at Selhausen. The value of $\overline{w'^2}/w_*^2$ would be less than 4 % higher in this case, i.e. the uncertainty in z_i does not explain the variability of a and the temporal variance.

Besides, some of the profiles with particularly high values of $\overline{w'^2}/w_*^2$ display a maximum at a height which is considerably above the average one at about $0.35z_i$. They are more similar to the profile of Sorbjan (1989, Fig. 11d). Caughey and Palmer (1979) also discuss the variability of heights of the variance maxima given by different authors. One assumption is that this is caused by strong thermals rising up to a certain height. Lenschow and Stephens (1980) developed a method for a sub-sampling of thermals from the time series of w and Lenschow and Stephens (1982) showed that the variance of thermals is 2–2.5 times higher than for the environment, depending on the

Variability of BL turbulence

V. Maurer et al.

Title Page

Abstract

Introduction

Conclusions

References

Tables

Figures

◀

▶

◀

▶

Back

Close

Full Screen / Esc

Printer-friendly Version

Interactive Discussion



method of calculation (the ratio is higher when the mean velocity of the sub-samples is subtracted before calculating the variance). Inspection of the time series of w for periods corresponding to the profiles with elevated w variance maxima (Fig. 11) reveals that these often contain strong convective cells. LES of van Heerwaarden et al. (2014) also support the finding that an elevated maximum of variance is related to particularly strong plumes.

Hence, it is concluded that local scaling, i.e. using the surface sensible heat flux from a single nearby station for the calculation of w_* , can lead to errors, especially when small-scale heterogeneity of the surface fluxes exists. This is reflected here by the large difference of the Bowen ratio between the two energy balance measurements of SE1 and Niederzier, which are less than 1.5 km apart. On the other hand the local scaling for one station (Wasserwerk) results in a much higher correlation than all other combinations. This means that it is possible for a single station to provide fluxes that are representative of the area influencing the CBL turbulence. Nevertheless, it can generally be assumed that the radius of influence and, thus, the area of representative w_* upstream of the measurements is several kilometers, depending on the mean wind and the convective time scale. When multiple energy balance measurements cannot be used, the representativeness of a single flux measurement site for scaling should be considered very carefully.

4.4 Influence of averaging periods and measurement uncertainties

The variance profiles considered so far were determined using hourly averaging periods. We now want to investigate how strongly the spatial differences are dependent on the length of the applied averaging periods. For this reason, the differences between $\overline{w'^2}_{\max}$ values at different locations were calculated for different averaging periods Δt . For the computation of variances for $\Delta t > 1$ h, the non-stationarity of the CBL, especially due to increasing z_i in the morning, has to be considered. For this, $\overline{w'^2}_{\max}$ values were first determined for the hourly averaging periods and then averaged to retrieve

$\overline{w'^2}_{\max}$ for longer averaging periods. After that, relative deviations (absolute difference normalized by the mean value) were calculated for each time step and each instrument combination. Finally, relative deviations were averaged for each day. The resulting mean relative differences are given as an average for all considered six days (Fig. 13a).
5 For the three days when simultaneous w measurements by HYB and WLS200 at the Wasserwerk were available (20, 22 and 24 April), the relative difference between these two measurements at the same site was calculated as well. This gives a good estimate for the uncertainty that exists due to the comparison of measurements by instruments that are based on different technologies or made by different manufacturers (instrument
10 uncertainty).

The daily mean relative deviation for HYB and WLS200 is less than 0.1 for $\Delta t = 1$ h and about 0.05 for longer averaging periods. For the other instrument combinations, it is about 0.5 for $\Delta t = 10$ min and decreases to about 0.2 for $\Delta t = 3$ h. For $\Delta t > 3$ h, it does not clearly decrease further. The mean normalized statistical error for $\Delta t = 3$ h is
15 about 0.1 (Fig. 13b), so that the relative deviation is about twice the error. This means that the spatial differences between the variances are not statistically significant on the average, at least if the instrument-to-instrument uncertainty is considered. However, this does not exclude the possibility of individual periods with significant spatial differences existing, as shown in Sect. 4.2; the diurnal time series of $\overline{w'^2}_{\max}$ with the
20 corresponding error bars were also compared for larger Δt and the significant differences for the periods concerned remained (not shown). At the same time, a mean relative deviation of about 0.2 for $\Delta t = 3$ h means that the mean error that has to be expected when calculating variances from point measurements is about 10 % minus the instrument uncertainty of about 2 % (a factor of 0.5 is taken into account to derive
25 the uncertainty of a single instrument from the calculated deviation); in other words, a point measurement is – on the average – spatially representative with an uncertainty of less than 10 % when a measurement period of three hours is covered. This agrees with the statistical error of Lenschow et al. (1994) that was derived by theoretical considerations.

Variability of BL turbulence

V. Maurer et al.

Title Page

Abstract

Introduction

Conclusions

References

Tables

Figures



Back

Close

Full Screen / Esc

Printer-friendly Version

Interactive Discussion



Variability of BL turbulence

V. Maurer et al.

Title Page

Abstract

Introduction

Conclusions

References

Tables

Figures



Back

Close

Full Screen / Esc

Printer-friendly Version

Interactive Discussion



As the absolute difference does not provide any evidence of possible biases between the instrument measurements, absolute values of $\overline{w'^2}_{\max}/w_*^2$ are compared in Fig. 13c. The variances were normalized by w_*^2 (averaged scaling) to retrieve comparable values for the different days. As for the normalized profiles (Fig. 11), the values mainly range from 0.25 to 0.5. While on the average they are as high at the Wasserwerk (HYB and WLS200) as at Hambach, most values are below the 1-1 diagonal for HALO. This explains why the relative difference is higher between HALO and both other instruments than between HYB and WTX (Fig. 13a). Nevertheless, there is no clear explanation why the variance is systematically smaller at Selhausen than 3 km north of this location. The sensible heat flux of SE1 mostly is quite low, but as shown in Sect. 4.3, it is not representative of the surroundings of the HALO site. Finally, to compare the daily differences, the absolute differences between the lidars were normalized by w_*^2 (Fig. 13d). The comparison reveals that on three days (18, 20, 22 April), the deviations are largest between HALO and WTX and on one day between HALO and HYB (24 April). On 4 May, which is the most perfect cloud-free day, all differences are smallest and on 19 May, which is a day with several mid-level clouds, they are largest. 19 May is the only day that falls into the wetter period with the Bowen ratio being low for all stations. Due to this, scaling with w_*^2 (using a small sensible heat flux) results in higher values than for the other days. The variation of the differences from day to day can, hence, partly be explained by the occurrence of clouds and therefore, by differences of the incoming radiation (Table 2).

For this section, we finally conclude that the spatial differences on the average are as large as the statistical error, which is derived from theory, and that this is independent of the averaging period. The instrument uncertainty can be estimated to about 2 % and the error is about 10 % for an averaging period of three hours.

4.5 Influence of the mean wind

Finally, we want to investigate the impact of the mean wind on spatial differences of the w variance, especially for periods when surface heterogeneities do not explain the differences and when differences do not disappear, even if the averaging interval amounts to several hours. For two of the three time periods investigated in Sect. 4.3.1 (on 18 and 24 April), the mean wind is from west to southwest. On both days, it is noticeable that the diurnal time series of $\overline{w'^2}_{\max}$ at Wasserwerk and Hambach are very similar (Fig. 7), while it is different at Selhausen (see also Fig. 13d). As the variances are similar, it can be expected that also the time series of w at Wasserwerk and Hambach exhibit a certain similarity. To investigate this, the cross correlation function of the two time series of w was determined (Fig. 14).

As the convective time scale t_* , also referred to as large-eddy turnover time, is of the order of 10 min and the travel time for the given distances between the lidar locations of about 3 km is between 4 and 12 min, convective cells can be preserved between two locations at least on days with relatively strong mean wind. This means that the original assumption that the w measurements were independent as long as they were more than 2 km apart turned out to be not valid for some days. The day with the strongest mean wind was 18 April; in the mean westerly flow, the WTX at Hambach is located downstream of WLS200 at the Wasserwerk. The cross correlation function between WLS200 and WTX in fact reveals a distinct maximum of correlation at a time lag of 200 s (Fig. 14a). The maximum correlation of 0.44 is found at heights between 500 and 900 m. When shifting the time series of w' at 600 m for WTX backwards by 200 s compared to that of WLS200, the two time series agree very well (Fig. 14a). That means that the larger convective cells are advected from the Wasserwerk to the Hambach site without substantial changing, which explains the similarity of the two time series of w and $\overline{w'^2}_{\max}$.

In contrast to 18 April, the mean wind direction on 20 April is northeast. On this day, large differences of $\overline{w'^2}_{\max}$ are observed between Hambach and Wasserwerk in the

Title Page

Abstract

Introduction

Conclusions

References

Tables

Figures



Back

Close

Full Screen / Esc

Printer-friendly Version

Interactive Discussion



afternoon. The cross correlation function (not shown) also shows very low correlations (< 0.1).

On 24 April, the mean wind again is from southwest, but weaker than on 18 April. A maximum of the cross correlation function between WLS200 and WTX can also be discerned (Fig. 14b), but it is only 0.27. Nevertheless, the two time series (WTX shifted by 400 s) at 700 m agree again very well, at least after 11:45 UTC. At the same time, the cross correlation mainly gives negative values, if it is calculated between the time series of vertical velocity for Selhausen and Hambach or between Selhausen and the Wasserwerk (not shown).

The mean wind direction may thus be a possible explanation why differences between the variances at Wasserwerk and at Hambach are found on 20 April, but not on 18 and 24 April (Fig. 7), although similar surface conditions exist on all of these days: the diurnal cycles of variances are similar at the two sites when the mean wind is parallel to their connecting axis, but different otherwise. For the time periods when the correlation between the two sites is high, the correlation between the third site and each of the two is low. It is remarkable that on 24 April, when convective cells are advected past Wasserwerk and Hambach without substantial changings, the mean vertical velocity (Fig. 15) is positive at Wasserwerk between 11:00–12:00 UTC (more than 1 ms^{-1}) and negative at Selhausen (11:00–13:00 UTC, i.e. even for two hours). We hypothesize that, while many cells are observed on the northern axis, less occur about 3 km further south due to the subsidence in the surroundings of the cells. This assumption is confirmed by model simulations for 24 April with the Consortium for Small-scale Modeling (COSMO) model in LES mode. They were performed on a grid with 100 m horizontal resolution using a 3-D-turbulence parameterization by Herzog et al. (2002). Model analyses of the operational model COSMO-DE (Baldauf et al., 2011) provided atmospheric initial and boundary conditions. The vertical velocity as calculated by the model is shown on a horizontal cross sections at 600 m (Fig. 16). About 1–1.5 km the south and north of the regions where the mean vertical velocity is positive on the hourly average, which is caused by convective cells advected with

Variability of BL turbulence

V. Maurer et al.

Title Page

Abstract

Introduction

Conclusions

References

Tables

Figures



Back

Close

Full Screen / Esc

Printer-friendly Version

Interactive Discussion



**Variability of BL
turbulence**

V. Maurer et al.

Title Page

Abstract

Introduction

Conclusions

References

Tables

Figures



Back

Close

Full Screen / Esc

Printer-friendly Version

Interactive Discussion



the mean wind, subsidence prevails. As shown by Lenschow and Stephens (1982), the mean w within thermals is positive and nearly two times higher than in the environment, where it is negative. This agrees very well with the mean w observed at the different locations on 24 April (Fig. 15). The spatial variance differences can therefore be explained by the occurrence of thermals: while more convective cells travel past the Wasserwerk as well as past Hambach, less occur near Selhausen. This structure is presumably the signature of horizontal rolls that develop during conditions of combined surface heating and strong winds (Stull, 1988, Ch. 11.2), as was observed by Brown (1970) or Kropfli and Kohn (1978).

5 Summary and conclusions

During the HOPE campaign, multiple Doppler lidars were operated simultaneously at three different sites in the vertical stare mode to retrieve temporally high-resolved vertical velocity measurements. For this study, vertical velocity variance profiles were derived for the three sites to investigate the spatial heterogeneity of turbulence in the cloud-free CBL. The aims were to compare, in a first step, the variance profiles for the different sites and to examine how large spatial differences were and, in a second step, to investigate if these differences were significant and if they depended on surface conditions, atmospheric conditions or on the averaging intervals.

The investigated area was characterized by patchy agricultural land use. The typical size of the crop fields was of the order of 100 m. The eight weeks of the measurement period were divided into a drier period (mid-April to 6 May) and a wetter one (starting on 7 May). It was found that the Bowen ratio varied between 0.5 and 4 during the drier period, while it was < 1 at all stations during the wetter period. Five of the six selected days fell into the drier period.

Boundary-layer mixing was strong on all of the selected days and the height of the CBL was between 1.2 and 2 km. Different methods to derive z_i agreed well. On three of the days, clouds occurred and the diurnal cycle of incoming radiation was slightly

Variability of BL turbulence

V. Maurer et al.

Title Page

Abstract

Introduction

Conclusions

References

Tables

Figures



Back

Close

Full Screen / Esc

Printer-friendly Version

Interactive Discussion



affected on 18 April, when some boundary-layer clouds occurred and on 19 May, when mid-level clouds were observed. Some cirrus clouds occurred on 24 April, but they did not perceptibly reduce incoming radiation. Moderate westerly wind dominated on most days; on 18 April, the mean wind was stronger than on the other days and it came from northeast on 20 April and 19 May.

The combination of smaller and larger Doppler lidars with complementary measurements at different range gates and heights above ground proved to be beneficial for the investigations. For the calculation of higher-order moments of w as measured by lidars, different aspects were considered: (1) the random noise of the signal (“uncorrelated noise”) was removed, (2) the lack of spectral contribution to the total energy caused by spatial averaging of the lidar measurement was neglected, and (3) the statistical errors (systematic and sampling error according to Lenschow et al., 1994) that appear due to the spatial and temporal sub-sampling were determined. Moreover, as measurements by lidar instruments from different manufacturers were compared here, also the instrument-dependent differences were calculated.

We found spatial differences of vertical velocity variances that were statistically significant. To investigate whether these differences were generated by heterogeneous surface conditions, scaling with the convective velocity w_* was applied. For the scaling, representative surface fluxes are needed. It is assumed that the relevant area for these has a side length of $t_*|\mathbf{v}| \approx 3\text{--}5$ km. This means that a sensible heat flux that is representative of the whole area and with this, a spatially representative w_* , should be most suitable for scaling. However, using the same values of w_* for all locations, only the temporal variability of the variances can be eliminated. Spatial differences can only be reduced by using different values of w_* for each location for scaling the variances. Both scaling methods were applied and the results imply that the spatial differences of the w variances can not be explained by the heterogeneity of the surface conditions. Moreover, scaled profiles for the whole data set showed large variations at the individual locations, which indicates that the local hourly heat supply is not the only factor influencing the w variance during the respective time interval in all cases. Apart from

**Variability of BL
turbulence**

V. Maurer et al.

Title Page

Abstract

Introduction

Conclusions

References

Tables

Figures



Back

Close

Full Screen / Esc

Printer-friendly Version

Interactive Discussion



that, it was found that in some cases, the nearby energy balance stations could not provide representative surface fluxes so that the use of weighted-averaged fluxes for the calculation of scaling variables was preferable in these cases. Only at one location was the temporal variability of w variance well related to the variability of w_* using the flux of the co-located energy balance station, with the correlation coefficient being 58 %. Lenschow et al. (2012) analyzed variance profiles for one location. As expected, the scatter around their mean value decreased after scaling, but a certain variation between values of 0.2 and 0.6 (for the vertical maximum) also remained. By removing the statistical error, they estimated that the real case-to-case variability was about 10 % and attributed it to the atmospheric stability which can be determined via the Obukhov length. However, the atmospheric stability can not be the main factor causing the case-to-case variability in this investigation, as only days with buoyancy-driven turbulence have been chosen.

Secondly, the influence of different averaging intervals on the spatial differences of w variance were analyzed. Relative deviations of w variances between all instruments averaged over all days were about as large as the relative statistical errors that can be derived from theoretical considerations (Lenschow et al., 1994) for all averaging intervals. Mean relative deviations as well as errors decreased strongly with increasing averaging intervals. Postulating that the uncertainty of a point measurement should not be larger than 10 %, measurement periods of at least 3 h – or hourly measurement periods of three instruments at different locations – are necessary. However, the uncertainty does not decrease much further for longer averaging intervals. Moreover, daily averages revealed that mean deviations were larger for days with a small number of clouds than on days with no clouds.

Finally, a varying degree of correlation between vertical velocity fluctuations existed for two locations on a east-west axis, depending on the mean wind speed. On 18 April, a day with stronger southwesterly wind, and on 24 April with moderate wind speed, the travel time was smaller than the large-eddy turnover time. On these days, fluctuations and variances were similar at the two locations, while the correlation of both with

Variability of BL turbulence

V. Maurer et al.

Title Page

Abstract

Introduction

Conclusions

References

Tables

Figures

◀

▶

◀

▶

Back

Close

Full Screen / Esc

Printer-friendly Version

Interactive Discussion



fluctuations at the third location about 2.5 km further south was low. It could be shown that for example on 24 April, the mean vertical velocity at the third location was negative for a time period of two hours, while it was positive at the other sites. The reason is that several convective cells travelled past the two northern sites, while subsidence prevailed at the third site during the whole 2 h period, which also explains why spatial variance differences do not disappear even for averaging periods of more than three hours. This is confirmed by LES.

Based on these findings, the following conclusions can be drawn: (1) The representativeness of single-column turbulence characteristics as observed by Doppler lidars is not necessarily given, even if long time periods are available (with the maximum possible length of the time period being the whole part of day with an existing CBL); (2) local scaling with w_* should only be considered, if the representativeness of a single energy balance station for a larger area is given; and (3) it is recommended to register turbulence profiles at more than one location – if Doppler lidar measurements are performed – to take the spatial variability of turbulence into account, which can depend on the relative location of the measurements compared to the mean wind direction.

Appendix A: Error statistics

A1 Uncorrelated noise

The so-called “uncorrelated noise” defined by Lenschow et al. (2000) is based on the assumption that the measurement signal is “contaminated by uncorrelated random noise”. By definition, it is uncorrelated from the signal and the error can, thus, be removed from the calculated variance. According to Eq. (8) from Lenschow et al. (2000), the error is equal to the difference between the first and zero lag of the autocovariance function.

A2 Systematic error

According to Lenschow et al. (1994), the statistical error can be separated into the systematic and the random error (see Appendix A3). The systematic error is caused by the fact that the variance $\overline{w'^2}$ derived from the measurement is, strictly speaking, a time average $\overline{w'^2}^t$, which is not equal to the ensemble average $\overline{w'^2}^{t,x}$. With these definitions, Eq. (14) from Lenschow et al. (1994) is

$$\frac{\overline{w'^2}^{t,x}}{\overline{w'^2}^t} \approx 1 - 2 \frac{\tilde{T}}{\Delta t}, \quad (\text{A1})$$

with the averaging time Δt and the integral time scale \tilde{T} (see Appendix B). The absolute error can, thus, be calculated as

$$\left| \overline{w'^2}^{t,x} - \overline{w'^2}^t \right| = \overline{w'^2}^t \cdot 2 \frac{\tilde{T}}{\Delta t}. \quad (\text{A2})$$

From this, it can be seen that the error decreases for increasing averaging periods and increases with the integral time scale.

A3 Random error

The random or sampling error takes into account that the length of the measured time series is not unlimited and that “random” time slots may differ. Lenschow et al. (1994) show that, using the error variance σ_2^2 for the second moment, the error can be approximated to

$$\sigma_2 = \overline{w'^2}^t \cdot \sqrt{2 \frac{\tilde{T}}{\Delta t}}. \quad (\text{A3})$$

Variability of BL
turbulence

V. Maurer et al.

Title Page

Abstract

Introduction

Conclusions

References

Tables

Figures



Back

Close

Full Screen / Esc

Printer-friendly Version

Interactive Discussion



The ratio of the systematic to the random error can, thus, be determined as $\sqrt{2\frac{\tilde{T}}{\Delta t}}$. For the commonly used averaging time of 1 h and a typical integral time scale of about 50 s (in this study, which agrees with numbers from Lothon et al., 2006, for example), this expression amounts to 0.17. This means that in this case, the random error is more than five times higher than the systematic error. Only for larger integral time scales, i.e. $\tilde{T} \geq 450$ s, does the systematic error become higher than the random error for the 1 h averaging period.

Appendix B: Integral time scale

Going back to Lumley and Panofsky (1964), the integral time scale is defined as the integral of the autocorrelation function R . Here, it was calculated as the integral between lag zero determined by extrapolation (Lenschow et al., 2000) and the first zero-crossing of R .

Acknowledgements. This work was funded by the Federal Ministry of Education and Research in Germany (BMBF) under the research program “High Definition Clouds and Precipitation for Climate Prediction – HD(CP)²” (FKZ: 01LK1212F). We want to thank Marius Schmidt from Forschungszentrum Jülich for providing surface fluxes from the energy balance stations that were operated within the framework of TERENO. Furthermore, Mauro Sulis and Prabhakar Shreshtha from University of Bonn provided the land-use data. Katja Träumner and the Young Investigator Group “Coherent structures” contributed to the operation of the Doppler lidars during the HOPE experiment and made their analysis tools available, including functions for error calculations. We are also grateful to the whole IMK team for their efforts in deploying KITcube.

The article processing charges for this open-access publication were covered by a Research Centre of the Helmholtz Association.

References

- Angevine, W. M., Doviak, R. J., and Sorbjan, Z.: Remote sensing of vertical velocity variance and surface heat flux in a convective boundary layer, *J. Appl. Meteorol.*, 33, 977–983, 1994. 18013
- 5 Ansmann, A., Fruntke, J., and Engelmann, R.: Updraft and downdraft characterization with Doppler lidar: cloud-free versus cumuli-topped mixed layer, *Atmos. Chem. Phys.*, 10, 7845–7858, doi:10.5194/acp-10-7845-2010, 2010. 18013
- Baldauf, M., Seifert, A., Förstner, J., Majewski, D., Raschendorfer, M., and Reinhardt, T.: Operational convective-scale numerical weather prediction with the COSMO model: description and sensitivities, *Mon. Weather Rev.*, 139, 3887–3905, 2011. 18035
- 10 Beyrich, F. and Mengelkamp, H.-T.: Evaporation over a heterogeneous land surface: EVA_GRIPS and the LITFASS-2003 experiment – an overview, *Bound.-Lay. Meteorol.*, 121, 5–32, doi:10.1007/s10546-006-9079-z, 2006. 18018
- Brown, R. A.: A secondary flow model for the planetary boundary layer, *J. Atmos. Sci.*, 27, 742–757, 1970. 18036
- 15 Browning, K. and Wexler, R.: The determination of kinematic properties of a wind field using Doppler radar, *J. Appl. Meteorol.*, 7, 105–113, 1968. 18016
- Brugger, P., Träumner, K., and Stawiarski, C.: Evaluation of a procedure to correct spatial averaging in turbulence statistics from a Doppler lidar by comparing time series with an ultrasonic anemometer, *J. Atmos. Ocean. Tech.*, submitted, 2015. 18020
- 20 Carbajo Fuertes, F., Iungo, G. V., and Porté-Agel, F.: 3D turbulence measurements using three synchronous wind LiDARs: validation against sonic anemometry, *J. Atmos. Ocean. Tech.*, 31, 1549–1556, doi:10.1175/JTECH-D-13-00206.1, 2014. 18021
- Caughey, S. J. and Palmer, S. G.: Some aspects of turbulence structure through the depth of the convective boundary layer, *Q. J. Roy. Meteor. Soc.*, 105, 811–827, doi:10.1002/qj.49710544606, 1979. 18013, 18030
- 25 Dardorff, J. W.: Preliminary results from numerical integrations of the unstable planetary boundary layer, *J. Atmos. Sci.*, 27, 1209–1211, 1970a. 18013, 18014
- Dardorff, J. W.: Convective velocity and temperature scales for the unstable planetary boundary layer and for Rayleigh convection, *J. Atmos. Sci.*, 27, 1211–1213, 1970b. 18030
- 30

Variability of BL turbulence

V. Maurer et al.

[Title Page](#)[Abstract](#)[Introduction](#)[Conclusions](#)[References](#)[Tables](#)[Figures](#)[⏪](#)[⏩](#)[◀](#)[▶](#)[Back](#)[Close](#)[Full Screen / Esc](#)[Printer-friendly Version](#)[Interactive Discussion](#)

**Variability of BL
turbulence**

V. Maurer et al.

Title Page

Abstract

Introduction

Conclusions

References

Tables

Figures



Back

Close

Full Screen / Esc

Printer-friendly Version

Interactive Discussion



- Deardorff, J. W.: Three-dimensional numerical study of the height and mean structure of a heated planetary boundary layer, *Bound.-Lay. Meteorol.*, 7, 81–106, doi:10.1007/BF00224974, 1974. 18013, 18024, 18030
- Eder, F., Schmidt, M., Damian, T., Träumner, K., and Mauder, M.: Mesoscale eddies affect near-surface turbulent exchange: evidence from lidar and tower measurements, *J. Appl. Meteorol.*, 54, 189–206, doi:10.1175/JAMC-D-14-0140.1, 2015. 18016
- Emeis, S., Schäfer, K., and Münkel, C.: Surface-based remote sensing of the mixing-layer height – a review, *Meteorol. Z.*, 17, 621–630, doi:10.1127/0941-2948/2008/0312, 2008. 18023
- Eng, K., Coulter, R. L., and Brutsaert, W.: Vertical velocity variance in the mixed layer from radar wind profilers, *J. Hydrol. Eng.*, 8, 301–307, 2003. 18013
- Eymard, L. and Weill, A.: Dual Doppler radar investigation of the tropical convective boundary layer, *J. Atmos. Sci.*, 45, 853–864, 1988. 18013
- Frehlich, R., Hannon, S., and Henderson, S.: Coherent Doppler lidar measurements of wind field statistics, *Bound.-Lay. Meteorol.*, 86, 233–256, doi:10.1023/A:1000676021745, 1998. 18020
- Graf, A., Schüttemeyer, D., Geiß, H., Knaps, A., Möllmann-Coers, M., Schween, J. H., Kollet, S., Neininger, B., Herbst, M., and Vereecken, H.: Boundedness of turbulent temperature probability distributions, and their relation to the vertical profile in the convective boundary layer, *Bound.-Lay. Meteorol.*, 134, 459–486, 2010. 18015
- Hadfield, M., Cotton, W., and Pielke, R.: Large-eddy simulations of thermally forced circulations in the convective boundary layer. Part I: A small-scale circulation with zero wind, *Bound.-Lay. Meteorol.*, 57, 79–114, doi:10.1007/BF00119714, 1991. 18013
- Herzog, H.-J., Vogel, G., and Schubert, U.: LLM – a nonhydrostatic model applied to high-resolving simulations of turbulent fluxes over heterogeneous terrain, *Theor. Appl. Climatol.*, 73, 67–86, doi:10.1007/s00704-002-0694-4, 2002. 18035
- Hogan, R. J., Grant, A. L., Illingworth, A. J., Pearson, G. N., and O'Connor, E. J.: Vertical velocity variance and skewness in clear and cloud-topped boundary layers as revealed by Doppler lidar, *Q. J. Roy. Meteor. Soc.*, 135, 635–643, 2009. 18013
- Kaimal, J., Wyngaard, J., Haugen, D., Coté, O., Izumi, Y., Caughey, S., and Readings, C.: Turbulence structure in the convective boundary layer, *J. Atmos. Sci.*, 33, 2152–2169, 1976. 18013

Variability of BL turbulence

V. Maurer et al.

Title Page

Abstract

Introduction

Conclusions

References

Tables

Figures



Back

Close

Full Screen / Esc

Printer-friendly Version

Interactive Discussion



- Kalthoff, N., Adler, B., Wieser, A., Kohler, M., Träumner, K., Handwerker, J., Corsmeier, U., Khodayar, S., Lambert, D., Kopmann, A., Kunka, N., Dick, G., Ramatschi, M., Wickert, J., and Kottmeier, Ch.: KITcube – a mobile observation platform for convection studies deployed during HyMeX, *Meteorol. Z.*, 22, 633–647, doi:10.1127/0941-2948/2013/0542, 2013. 18015
- 5 Kropfli, R. and Kohn, N.: Persistent horizontal rolls in the urban mixed layer as revealed by dual-Doppler radar, *J. Appl. Meteorol.*, 17, 669–676, 1978. 18036
- Lenschow, D. H. and Stankov, B. B.: Length scales in the convective boundary layer, *J. Atmos. Sci.*, 43, 1198–1209, 1986. 18013, 18014
- Lenschow, D. H. and Stephens, P. L.: The role of thermals in the convective boundary layer, *Bound.-Lay. Meteorol.*, 19, 509–532, doi:10.1007/BF00122351, 1980. 18030
- 10 Lenschow, D. H. and Stephens, P. L.: Mean vertical velocity and turbulence intensity inside and outside thermals, *Atmos. Environ.*, 16, 761–764, doi:10.1016/0004-6981(82)90393-6, 1982. 18030, 18036
- Lenschow, D. H., Wyngaard, J. C., and Pennell, W. T.: Mean-field and second-moment budgets in a baroclinic, convective boundary layer, *J. Atmos. Sci.*, 37, 1313–1326, 1980. 18013, 18014, 18023, 18024, 18029, 18057
- 15 Lenschow, D. H., Mann, J., and Kristensen, L.: How long is long enough when measuring fluxes and other turbulence statistics?, *J. Atmos. Ocean. Tech.*, 11, 661–673, 1994. 18013, 18014, 18022, 18032, 18037, 18038, 18040, 18055, 18057
- Lenschow, D. H., Wulfmeyer, V., and Senff, C.: Measuring second-through fourth-order moments in noisy data, *J. Atmos. Ocean. Tech.*, 17, 1330–1347, 2000. 18022, 18039, 18041
- Lenschow, D. H., Lothon, M., Mayor, S. D., Sullivan, P. P., and Canut, G.: A comparison of higher-order vertical velocity moments in the convective boundary layer from lidar with in situ measurements and large-eddy simulation, *Bound.-Lay. Meteorol.*, 143, 107–123, 2012. 20 18013, 18038
- Lothon, M., Lenschow, D. H., and Mayor, S.: Coherence and scale of vertical velocity in the convective boundary layer from a Doppler lidar, *Bound.-Lay. Meteorol.*, 121, 521–536, doi:10.1007/s10546-006-9077-1, 2006. 18041
- 25 Lothon, M., Lenschow, D. H., and Mayor, S. D.: Doppler lidar measurements of vertical velocity spectra in the convective planetary boundary layer, *Bound.-Lay. Meteorol.*, 132, 205–226, 2009. 18013
- 30

Variability of BL
turbulence

V. Maurer et al.

Title Page

Abstract

Introduction

Conclusions

References

Tables

Figures



Back

Close

Full Screen / Esc

Printer-friendly Version

Interactive Discussion



- Lumley, J. L. and Panofsky, H. A.: The Structure of Atmospheric Turbulence, Interscience Monographs and Texts in Physics and Astronomy; 12, Interscience Publ., New York, NY, 239 pp., 1964. 18041
- Mahrt, L.: Flux sampling errors for aircraft and towers, *J. Atmos. Ocean. Tech.*, 15, 416–429, 1998. 18014
- 5 Mauder, M. and Foken, T.: Documentation and instruction manual of the eddy-covariance software package TK3, *Abteilung Mikrometeorologie: Arbeitsergebnisse* 46, ISSN 1614-8924, 60 pp., 2011. 18017
- Mauder, M., Cuntz, M., Drüe, C., Graf, A., Rebmann, C., Schmid, H. P., Schmidt, M., and Steinbrecher, R.: A strategy for quality and uncertainty assessment of long-term eddy-covariance measurements, *Agr. Forest Meteorol.*, 169, 122–135, doi:10.1016/j.agrformet.2012.09.006, 2013. 18017
- 10 Moeng, C.-H.: A large-eddy-simulation model for the study of planetary boundary-layer turbulence, *J. Atmos. Sci.*, 41, 2052–2062, 1984. 18013
- Neggers, R. A. J., Duynkerke, P. G., and Rodts, S. M. A.: Shallow cumulus convection: a validation of large-eddy simulation against aircraft and Landsat observations, *Q. J. Roy. Meteor. Soc.*, 129, 2671–2696, doi:10.1256/qj.02.93, 2003. 18027
- Panofsky, H. and Mazzola, C.: Variances and spectra of vertical velocity just above the surface layer, *Bound.-Lay. Meteorol.*, 2, 30–37, 1971. 18013
- 20 Pearson, G., Davies, F., and Collier, C.: An analysis of the performance of the UFAM pulsed Doppler lidar for observing the boundary layer, *J. Atmos. Ocean. Tech.*, 26, 240–250, 2009. 18016
- Pospichal, B. and Crewell, S.: Boundary layer observations in West Africa using a novel microwave radiometer, *Meteorol. Z.*, 16, 513–523, doi:10.1127/0941-2948/2007/0228, 2007. 18018
- 25 Schröter, M., Bange, J., and Raasch, S.: Simulated airborne flux measurements in a LES generated convective boundary layer, *Bound.-Lay. Meteorol.*, 95, 437–456, doi:10.1023/A:1002649322001, 2000. 18014
- Sorbjan, Z.: On similarity in the atmospheric boundary layer, *Bound.-Lay. Meteorol.*, 34, 377–397, doi:10.1007/BF00120989, 1986. 18014
- 30 Sorbjan, Z.: Local similarity in the convective boundary layer (CBL), *Bound.-Lay. Meteorol.*, 45, 237–250, doi:10.1007/BF01066672, 1988. 18013

Variability of BL
turbulence

V. Maurer et al.

Title Page

Abstract

Introduction

Conclusions

References

Tables

Figures

◀

▶

◀

▶

Back

Close

Full Screen / Esc

Printer-friendly Version

Interactive Discussion



- Sorbjan, Z.: Structure of the Atmospheric Boundary Layer, Prentice Hall, Englewood Cliffs, New Jersey, 317 pp., 1989. 18013, 18023, 18030
- Steinfeld, G., Letzel, M., Raasch, S., Kanda, M., and Inagaki, A.: Spatial representativeness of single tower measurements and the imbalance problem with eddy-covariance fluxes: results of a large-eddy simulation study, *Bound.-Lay. Meteorol.*, 123, 77–98, doi:10.1007/s10546-006-9133-x, 2007. 18014
- Stull, R. B.: An Introduction to Boundary Layer Meteorology, Atmospheric Sciences Library; 13, Kluwer, Dordrecht, the Netherlands [u.a.], 666 pp., 1988. 18025, 18036
- Träumner, K., Kottmeier, C., Corsmeier, U., and Wieser, A.: Convective boundary-layer entrainment: short review and progress using Doppler lidar, *Bound.-Lay. Meteorol.*, 141, 369–391, doi:10.1007/s10546-011-9657-6, 2011. 18016, 18022, 18023
- Tucker, S. C., Senff, C. J., Weickmann, A. M., Brewer, W. A., Banta, R. M., Sandberg, S. P., Law, D. C., and Hardesty, R. M.: Doppler lidar estimation of mixing height using turbulence, shear, and aerosol profiles, *J. Atmos. Ocean. Tech.*, 26, 673–688, doi:10.1175/2008JTECHA1157.1, 2009. 18023
- van Heerwaarden, C. C., Mellado, J. P., and De Lozar, A.: Scaling laws for the heterogeneously heated free convective boundary layer, *J. Atmos. Sci.*, 71, 3975–4000, doi:10.1175/JAS-D-13-0383.1, 2014. 18031
- Warner, J.: The structure and intensity of turbulence in air over the sea, *Q. J. Roy. Meteor. Soc.*, 98, 175–186, doi:10.1002/qj.49709841514, 1972. 18013
- Willis, G. and Deardorff, J.: A laboratory model of the unstable planetary boundary layer, *J. Atmos. Sci.*, 31, 1297–1307, 1974. 18013, 18014
- Wyngaard, J., Coté, O., and Izumi, Y.: Local free convection, similarity, and the budgets of shear stress and heat flux, *J. Atmos. Sci.*, 28, 1171–1182, 1971. 18013
- Young, G. S.: Turbulence structure of the convective boundary layer. Part I. Variability of normalized turbulence statistics, *J. Atmos. Sci.*, 45, 719–726, 1988. 18013
- Zacharias, S., Bogen, H., Samaniego, L., Mauder, M., Fuß, R., Pütz, T., Frenzel, M., Schwank, M., Baessler, C., Butterbach-Bahl, K., Bens, O., Borg, E., Brauer, A., Dietrich, P., Hajsek, I., Helle, G., Kiese, R., Kunstmann, H., Klotz, S., Munch, J. Ch., Papen, H., Priesack, E., Schmid, H. P., Steinbrecher, R., Rosenbaum, U., Teutsch, G., and Vereecken, H.: A network of terrestrial environmental observatories in Germany, *Vadose Zone J.*, 10, 955–973, doi:10.2136/vzj2010.0139, 2011. 18015

Variability of BL turbulence

V. Maurer et al.

Title Page

Abstract

Introduction

Conclusions

References

Tables

Figures

◀

▶

◀

▶

Back

Close

Full Screen / Esc

Printer-friendly Version

Interactive Discussion



Table 1. Overview of lidar instruments at the three sites, with abbreviations used in the text, measurement range r for the vertical stare mode, range-gate length Δr , and applied threshold of signal-to-noise ratio (SNR; w measurements with SNR below the threshold were not used in this study).

lidar	HYB	WLS200	HALO	WTX	WLS7
location	Wasserwerk	Wasserwerk	Selhausen	Hambach	Hambach
specification	WindTracer	WINDCUBE 200S	Stream Line	WindTracer	WindCube v2
manufacturer	Lockheed Martin CT	Leosphere	Halo Photonics	Lockheed Martin CT	Leosphere
r in m a.g.l.	350 – above CBL top	50 – CBL top	60 – CBL top	350 – CBL top	40–290
Δr in m	≈ 60	25	18	≈ 60	25
SNR threshold in dBZ	–8	–26	–16	–8	–22

Variability of BL turbulence

V. Maurer et al.

Table 2. Overview of characteristic mean values and scales for all considered days: Diurnal maximum of surface sensible heat flux H_0 and of boundary-layer height z_i ; daily mean values of integrated water vapor IWV, of spatial mean and standard deviation of incoming shortwave radiation $Q_{SW,in}$, of mean boundary-layer wind speed $|\mathbf{v}|$, and of wind direction; diurnal maximum of convective velocity scale w_* and corresponding convective time scale t_* ; diurnal mean of $\overline{w'^2}_{max}$ and of integral time scale \tilde{T} (instrument mean); estimated peak wavelength of turbulence spectra in 600 m height (10:00–17:00 UTC), $\lambda_{p,w} = |\mathbf{v}|f_{p,w}^{-1}$ (using Taylor's hypothesis), with time period $T = f_{p,w}^{-1}$, and period T of the autocorrelation function with corresponding wavelength λ (denoted as n/a when no estimation was possible).

	18/04	20/04	22/04	24/04	04/05	19/05
$ \mathbf{v} $ in m s^{-1}	12	8	4	5	8	5
wind dir. in $^\circ$	250	45	270	270	270	0–90
IWV in kg m^{-2}	12	8	8	20	10	10
$Q_{SW,in}$ in W m^{-2}	460	490	510	520	560	580
$\sigma(Q_{SW,in})$ in W m^{-2}	100	60	30	60	30	90
H_0 in W m^{-2}	200	210	180	180	200	90
z_i in m	2030	1350	1900	1330	1280	1250
peak wavelength from spectra:						
T in min	n/a	5.5	8	8	5	n/a
$\lambda_{p,w}$ in km	n/a	2.7	2	2.5	2	n/a
period of autocorrelation function:						
T in min	n/a	6–10	15	10	n/a	6
λ in km	n/a	2.8–4.4	3.6	3	n/a	1.8
$\overline{w'^2}_{max}$ in $\text{m}^{-2} \text{s}^{-2}$	1.65	1.55	1.2	0.95	1.1	1.05
w_* in m s^{-1}	2.24	1.98	2.02	1.82	1.93	1.39
t_* in min	15	11	16	12	11	15
\tilde{T} in s	40	47	55	56	40	45

Title Page

Abstract

Introduction

Conclusions

References

Tables

Figures

◀

▶

◀

▶

Back

Close

Full Screen / Esc

Printer-friendly Version

Interactive Discussion



Variability of BL turbulence

V. Maurer et al.

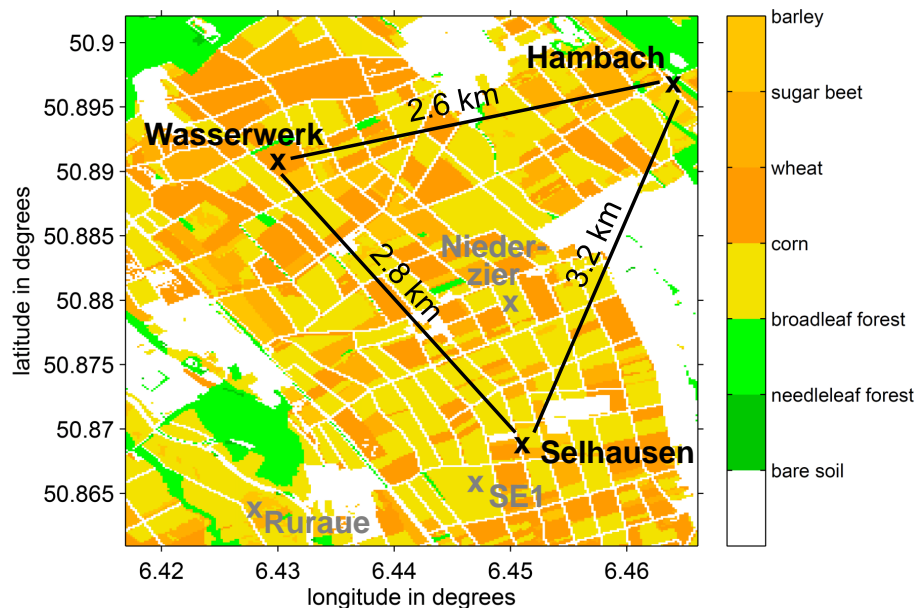


Figure 1. Land-use classification with positions of energy balance stations and lidars at Hambach and Wasserwerk and of the lidar at Selhausen (black crosses) as well as of the TERENO energy balance stations at Ruraue, near Selhausen (SE1), and at Niederzier (gray crosses); black lines denote the relative lidar locations.

Title Page

Abstract

Introduction

Conclusions

References

Tables

Figures

◀

▶

◀

▶

Back

Close

Full Screen / Esc

Printer-friendly Version

Interactive Discussion



Variability of BL turbulence

V. Maurer et al.

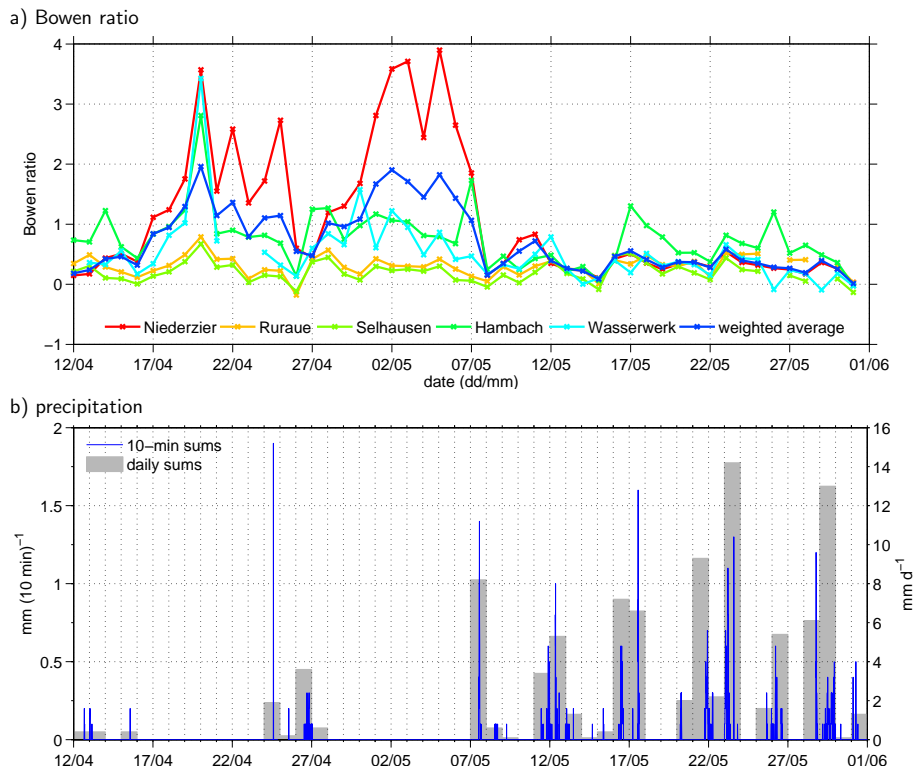


Figure 2. Bowen ratio for all energy balance stations as well as for the weighted-averaged fluxes (weighted with the area fraction of each land-use class), calculated from daily averaged values of surface fluxes for 09:00–15:00 UTC (a) and precipitation from rain gauge measurements at Wasserwerk (b).



Variability of BL turbulence

V. Maurer et al.

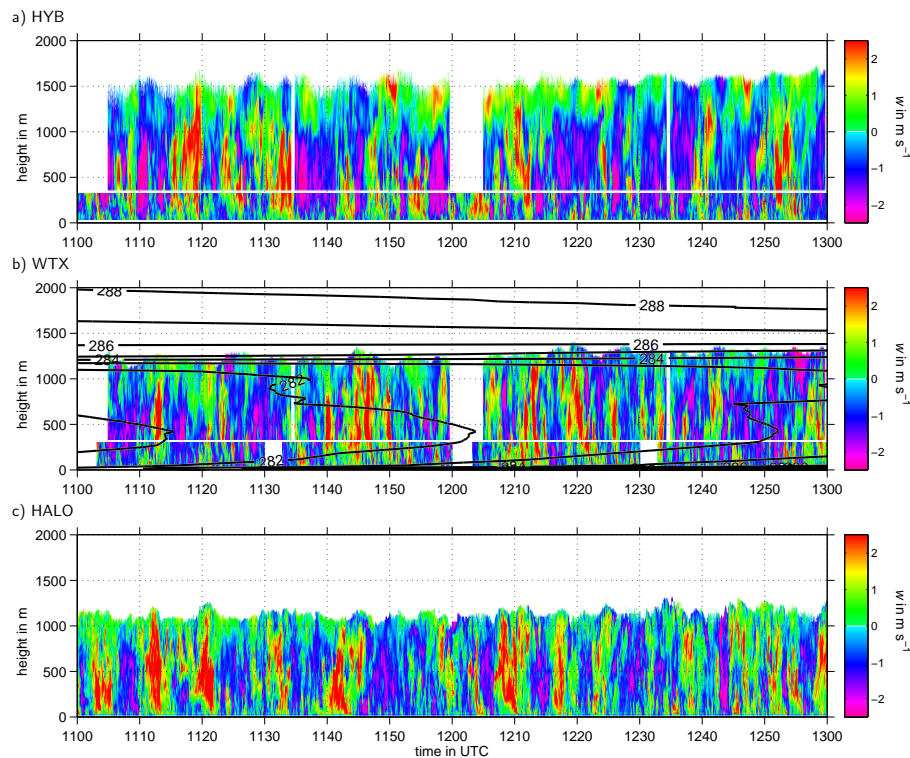


Figure 3. Vertical velocity as observed by Doppler lidars at three different locations on 20 April 2013 (11:00–13:00 UTC) with isolines of potential temperature (in K) in **(b)** as derived from radiosoundings.

[Title Page](#)[Abstract](#)[Introduction](#)[Conclusions](#)[References](#)[Tables](#)[Figures](#)[Back](#)[Close](#)[Full Screen / Esc](#)[Printer-friendly Version](#)[Interactive Discussion](#)

Variability of BL turbulence

V. Maurer et al.

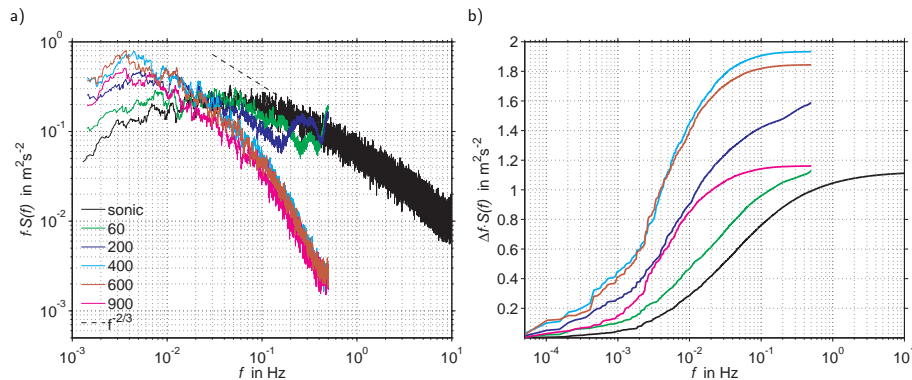


Figure 4. (a) Turbulence spectra of w measurements at Hambach on 20 April 2013, 09:00–15:00 UTC, from an ultrasonic at 30 m, WLS7 (60 and 200 m), and WTX (400, 600, 900 m); additionally, the theoretical slope in the inertial subrange is given; (b) as in (a) but accumulated curves to illustrate the contributions of different frequencies to the variance.

Variability of BL turbulence

V. Maurer et al.

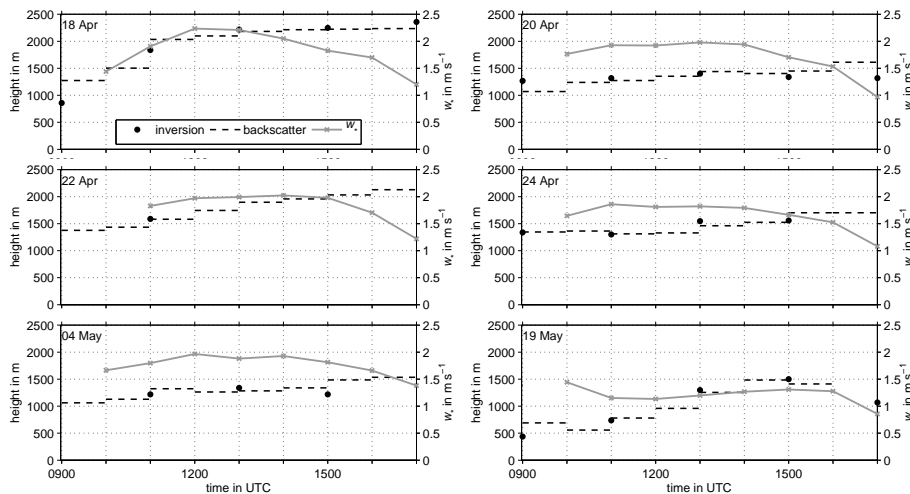


Figure 5. Boundary-layer heights derived from radiosoundings (maximum temperature gradient = inversion) and from lidar backscatter data (W_t) for all considered cloud-free days; additionally, the convective velocity scale w_* (determined using weighted-averaged values of sensible heat flux) is given.

Title Page

Abstract

Introduction

Conclusions

References

Tables

Figures



Back

Close

Full Screen / Esc

Printer-friendly Version

Interactive Discussion



Variability of BL turbulence

V. Maurer et al.

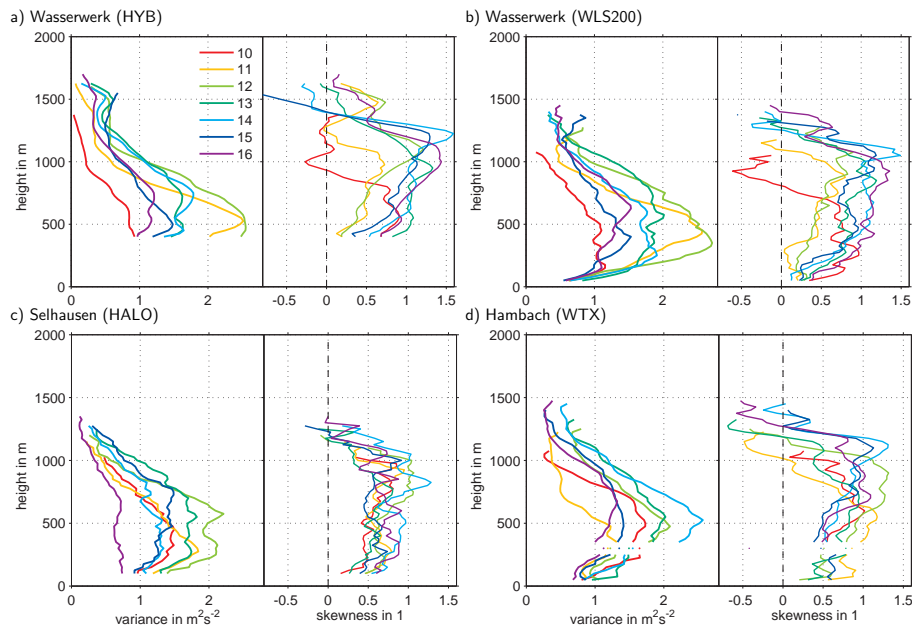


Figure 6. Vertical profiles of hourly vertical velocity variance and skewness from lidar measurements at the three locations for 10:00–17:00 UTC on 20 April 2013; the legend labels in (a) refer to the end in UTC for each averaging period of 60 min.

Title Page

Abstract

Introduction

Conclusions

References

Tables

Figures



Back

Close

Full Screen / Esc

Printer-friendly Version

Interactive Discussion



Variability of BL turbulence

V. Maurer et al.

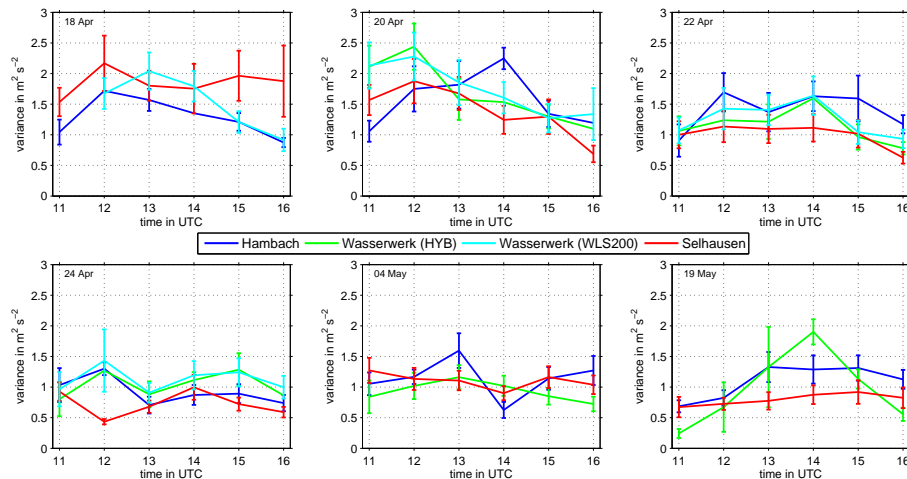


Figure 7. Vertical velocity variances (hourly profiles averaged over $z_{\max} \pm 250$ m) at the three locations with error bars displaying the statistical error according to Lenschow et al. (1994) for all six days (different panels).

Title Page

Abstract

Introduction

Conclusions

References

Tables

Figures



Back

Close

Full Screen / Esc

Printer-friendly Version

Interactive Discussion



Variability of BL turbulence

V. Maurer et al.

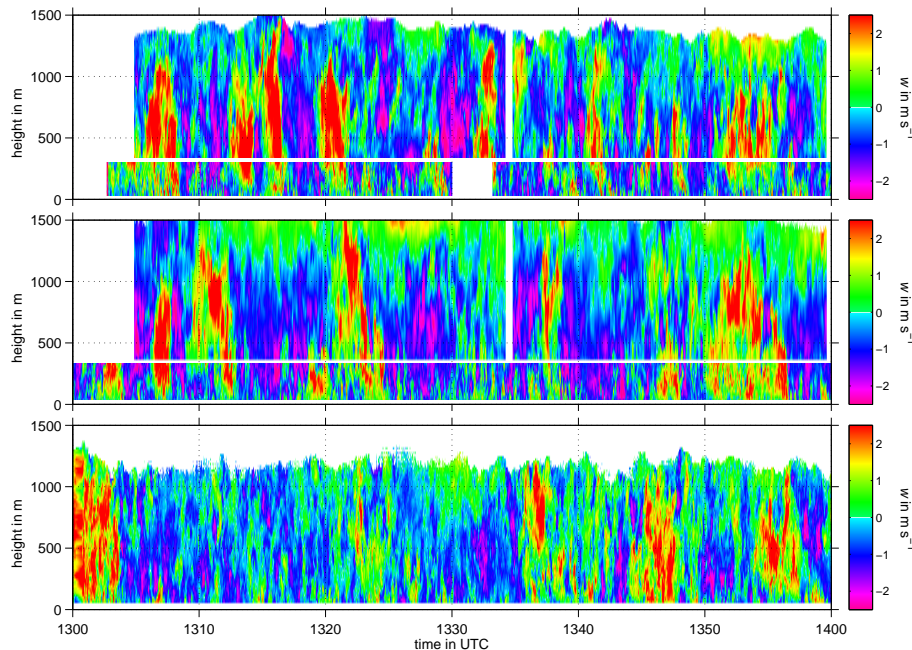


Figure 8. Time series of vertical velocity at Hambach, Wasserwerk, and Selhausen (from top to bottom) on 20 April, 13:00–14:00 UTC.

[Title Page](#)[Abstract](#)[Introduction](#)[Conclusions](#)[References](#)[Tables](#)[Figures](#)[⏪](#)[⏩](#)[◀](#)[▶](#)[Back](#)[Close](#)[Full Screen / Esc](#)[Printer-friendly Version](#)[Interactive Discussion](#)

Variability of BL turbulence

V. Maurer et al.

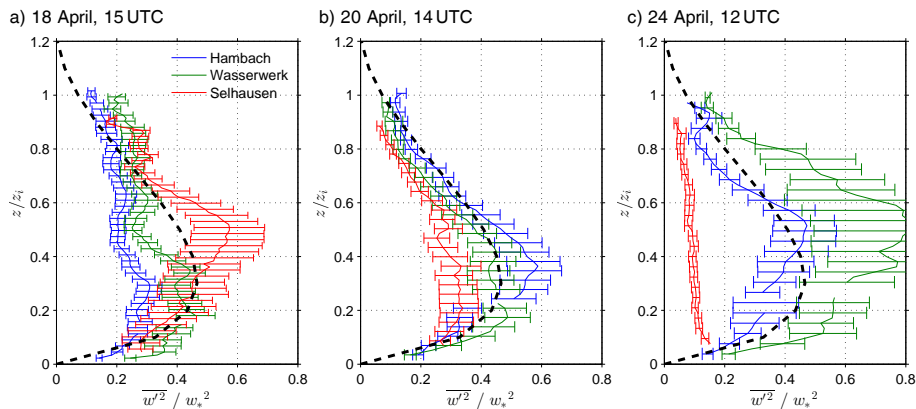


Figure 9. Normalized variance profiles with error bars (statistical error according to Lenschow et al., 1994) for three time periods; the black dashed line corresponds to the fit of Lenschow et al. (1980), Eq. (1).

[Title Page](#)[Abstract](#)[Introduction](#)[Conclusions](#)[References](#)[Tables](#)[Figures](#)[Back](#)[Close](#)[Full Screen / Esc](#)[Printer-friendly Version](#)[Interactive Discussion](#)

Variability of BL turbulence

V. Maurer et al.

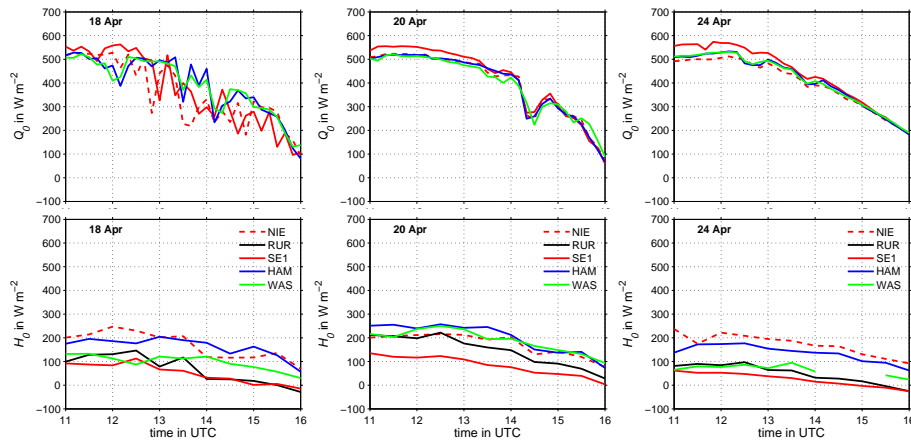


Figure 10. Net radiation (Q_0 , upper row) and surface sensible heat flux (H_0) at the five energy balance stations (NIE – Niederzier; RUR – Ruraue; SE1 – Selhausen; HAM – Hambach; WAS – Wasserwerk, cf. Fig. 1) for three days with significant spatial differences of vertical velocity variances.

Title Page

Abstract

Introduction

Conclusions

References

Tables

Figures

◀

▶

◀

▶

Back

Close

Full Screen / Esc

Printer-friendly Version

Interactive Discussion



Variability of BL turbulence

V. Maurer et al.

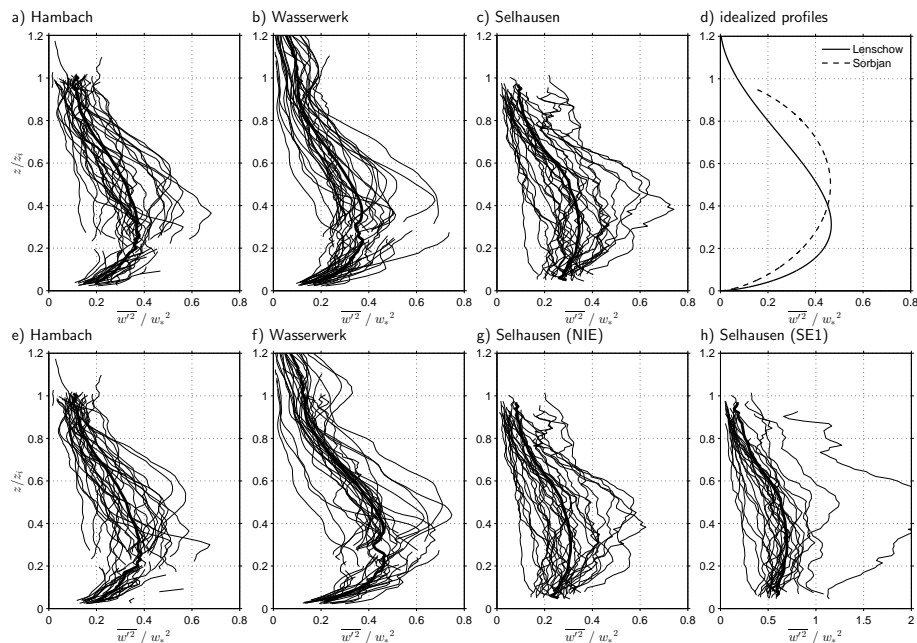


Figure 11. Normalized hourly variance profiles for 18, 20, 22, 24 April and 04 May (11:00–16:00 UTC), with averaged (**a**, **b**, **c**) and local scaling (**e**, **f**, **g**, **h**) for each location; different energy balance stations were used for scaling in (**g**) and (**h**); in (**d**), the idealized profiles according to Eq. (1) are given.



Variability of BL turbulence

V. Maurer et al.

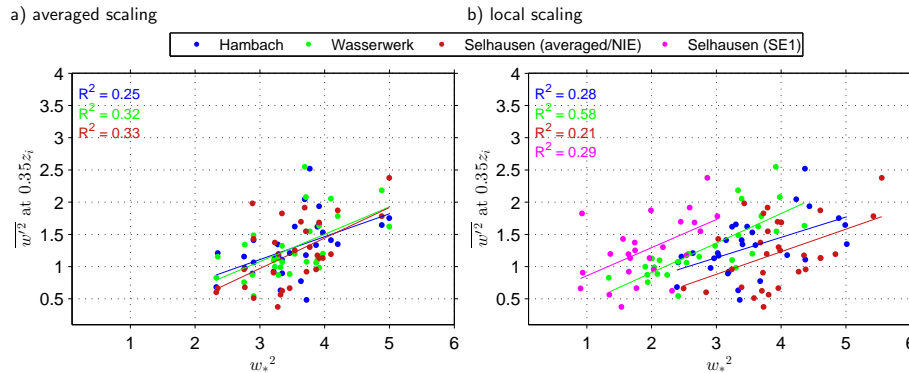


Figure 12. Vertical velocity variance at $0.35 z_i$ over w_*^2 , calculated using the weighted-averaged fluxes **(a)** and fluxes of nearby stations **(b)** for all time steps as in Fig. 11, with lines of best fit from linear regression and squared correlation coefficients R^2 .

Title Page

Abstract Introduction

Conclusions References

Tables Figures

◀ ▶

◀ ▶

Back Close

Full Screen / Esc

Printer-friendly Version

Interactive Discussion



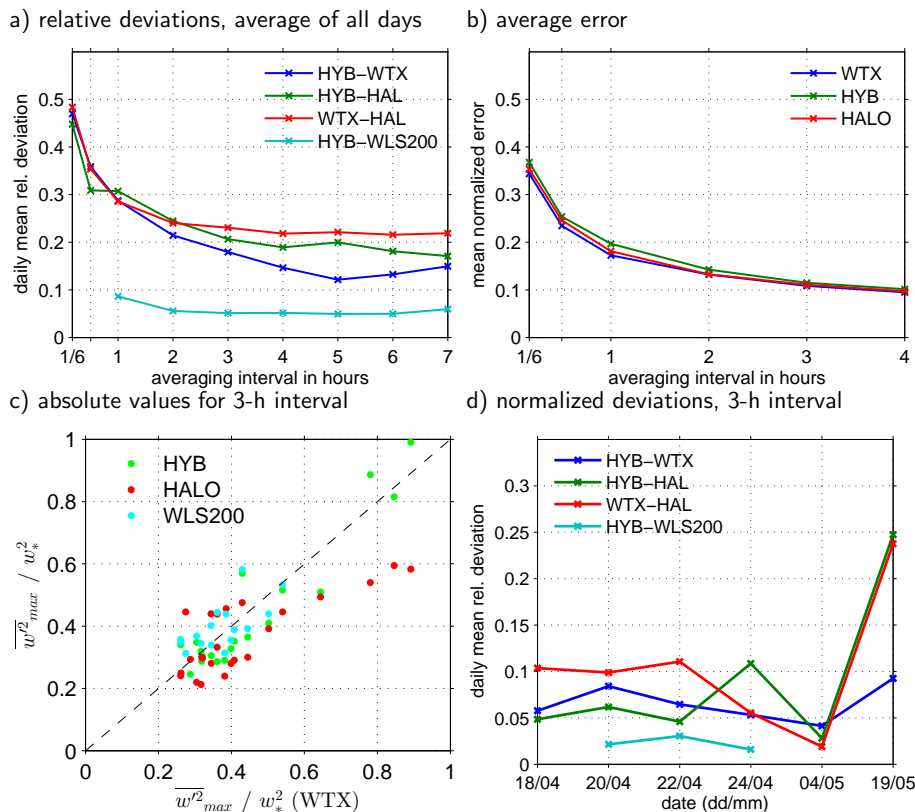


Figure 13. Relative deviations between $\overline{w'^2}_{max}$ time series of each two lidars, averaged daily and over all days **(a)** and statistical error for each instrument, normalized with the respective $\overline{w'^2}_{max}$ time series **(b)**, given as a function of the averaging interval used for the calculation of the variance profiles; absolute values of $\overline{w'^2}_{max} / w_*^2$ for the 3h averaging interval for HYB, HALO, and WLS200 as a function of $\overline{w'^2}_{max} / w_*^2$ for WTX **(c)**; deviation normalized with w_*^2 for 3h averaging interval for each day **(d)**.

Title Page	
Abstract	Introduction
Conclusions	References
Tables	Figures
◀	▶
◀	▶
Back	Close
Full Screen / Esc	
Printer-friendly Version	
Interactive Discussion	



Variability of BL turbulence

V. Maurer et al.

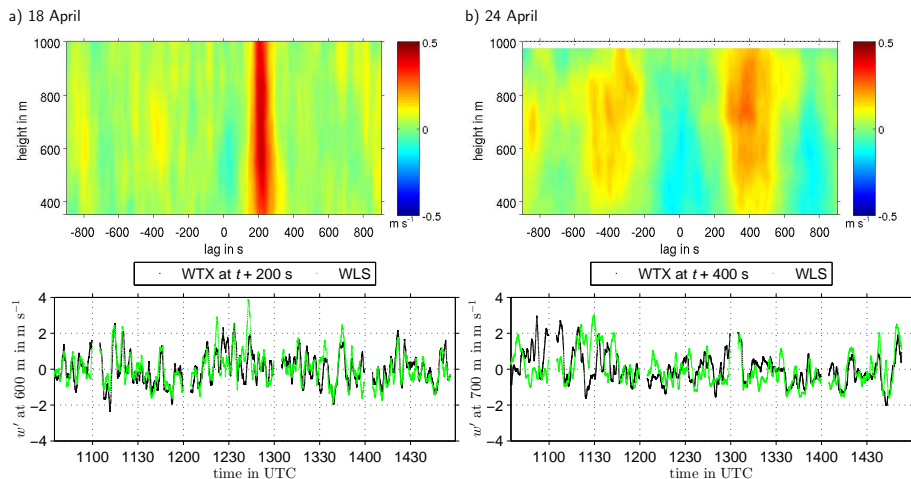


Figure 14. Cross correlation functions between w' time series (10:30–15:00 UTC) at Hambach and Wasserwerk (WTX and WLS200, respectively) for all range gates between 380 and 1000 m (upper row) and w' time series (± 50 s running average) for both lidars at one range gate (lower row) on 18 April (a) and 24 April 2013 (b).



Variability of BL turbulence

V. Maurer et al.

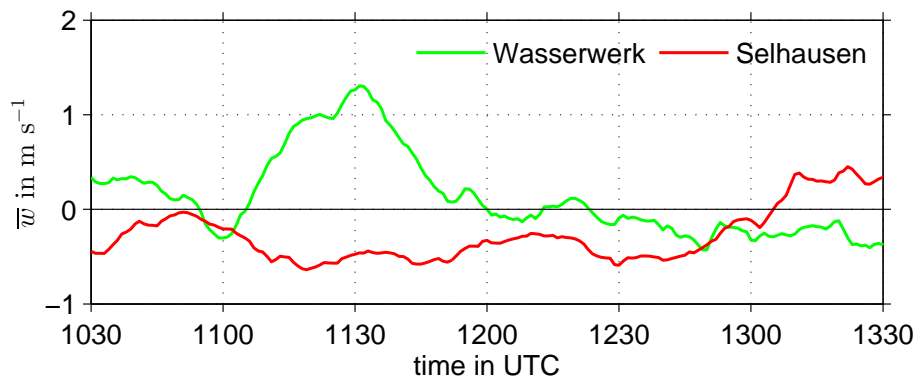


Figure 15. Mean vertical velocity (running average of 60 min) at 700 m (± 1 range gate) at Wasserwerk and Selhausen on 24 April.

[Title Page](#)[Abstract](#)[Introduction](#)[Conclusions](#)[References](#)[Tables](#)[Figures](#)[◀](#)[▶](#)[◀](#)[▶](#)[Back](#)[Close](#)[Full Screen / Esc](#)[Printer-friendly Version](#)[Interactive Discussion](#)

Variability of BL turbulence

V. Maurer et al.

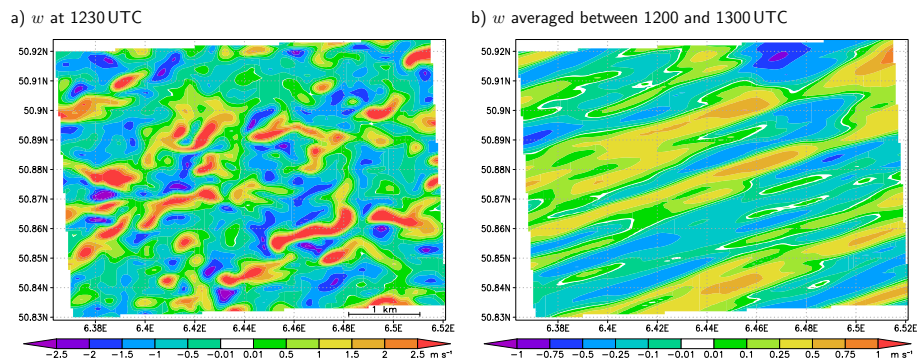


Figure 16. Vertical velocity at 600 m on 24 April 2013 from LES model output.

[Title Page](#)[Abstract](#)[Introduction](#)[Conclusions](#)[References](#)[Tables](#)[Figures](#)[◀](#)[▶](#)[◀](#)[▶](#)[Back](#)[Close](#)[Full Screen / Esc](#)[Printer-friendly Version](#)[Interactive Discussion](#)